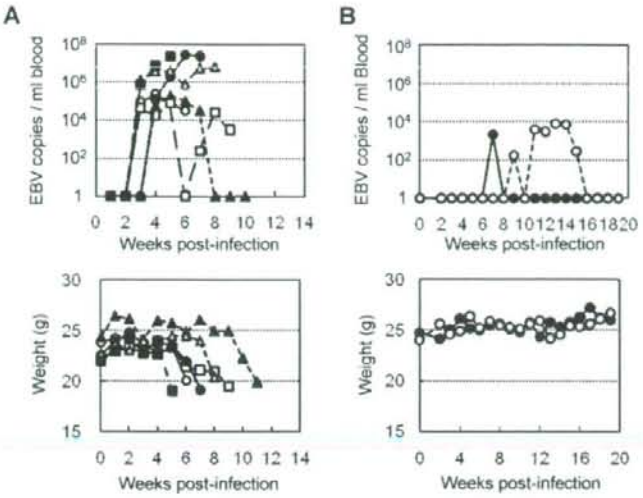

Figure 1. Peripheral blood Epstein-Barr virus (EBV) DNA load and body weight in humanized NOG (hNOG) mice infected with EBV. *A*, Infection at a high dose of virus. Six mice were inoculated intravenously with 1×10^3 TD_{50} of EBV. Peripheral blood EBV DNA load *(upper panels)* and body weight *(lower panels)* were then determined weekly. Each symbol in the graphs represents an individual mouse. Interruption of records indicates the death or killing of a mouse. *B*, Infection at lower doses. Peripheral blood EBV DNA load *(upper panel)* and body weight *(lower panel)* of 2 mice inoculated with low doses of EBV (*black circle*, 1×10^{-1} TD_{50}; *white circle*, 1×10^1 TD_{50}) are shown.

of 2×10^5 cells per well in 6-well plates and then inoculated with serial 10-fold dilutions of virus preparation. The number of wells with proliferating lymphocytes was counted 6 weeks after infection, and the titer of the virus in 50% transforming dose (TD_{50}) was determined by the Reed-Muench method [22]. EBV was inoculated intravenously through the tail vein. EBV DNA was quantified by a real-time quantitative polymerase chain reaction (PCR) assay based on the TaqMan system (Applied Biosystems), as described elsewhere [23]. Analysis of EBV gene expression by reverse-transcription PCR (RT-PCR) was done as described elsewhere, using the primers listed in table 1 [24].

Histopathology, in situ hybridization (ISH), and immunohistochemistry. Tissue samples were fixed in 10% buffered formalin, embedded in paraffin, and stained with hematoxylin-eosin. For phenotypic analysis of proliferating lymphocytes, immunostaining for CD3 (Nichirei), CD4 (Novocastra), CD8 (Nichirei), CD45RO, CD20, CD79a, CD30, Mum1 (Dako), CD23, CD10, CD56 (Novocastra), granzyme B (Dako), and T cell intracellular antigen 1 (Beckman Coulter) was performed on paraffin sections. EBV was detected by immunostaining for LMP1 and EBNA2 (Dako) and by ISH with EBV-encoded small RNA (EBER) probe. Immunohistochemistry and ISH were performed on an automated stainer (Benchmark XT; Ventana Medical Systems), in accordance with the manufacturer's recommendations. To determine the cell lineage of EBV-infected cells, paraffin sections were applied to double staining with EBER ISH and immunohistochemistry.

Detection of EBV-specific T cell response. Enzyme-linked immunospot (ELISPOT) assay was performed with the Immunocyto IFN-γ ELISPOT Kit (MBL), in accordance with the instructions supplied by the manufacturer. Briefly, $CD8^-$ T cells were isolated from PBMCs from EBV-infected hNOG mice with the IMag anti-human CD8 Particles–DM (BD Biosciences). Mixture of these $CD8^+$ T cells and an autologous LCL were incubated with interleukin (IL)–2 in microplates coated with antibody to interferon (IFN)–γ for 17 h. Captured IFN-γ was detected by use of biotinated antibody to IFN-γ and alkaline phosphatase–conjugated streptavidin and was visualized by reaction with the BCIP/NBT chromogen substrate. The unpaired Student's *t* test was used for statistical analysis. IFN-γ secretion in response to EBV was also examined by flow cytometry, as described elsewhere [25]. Briefly, aliquots of murine splenocytes and an LCL were mixed in 6-well plates in the presence of brefeldin A (10 μg/mL) and incubated at 37°C in 5% CO_2 for 17 h. After incubation, the cell suspensions were stained with phycoerythrin-conjugated anti-human CD69, phycoerythrin–Texas red–conjugated anti-human CD45, and phycoerythrin–cyanin 5–conjugated anti-human CD8 for 30 min at 4°C and were fixed with 2% paraformaldehyde. Cells were then permeabilized and stained with BD Perm/Wash buffer (BD Biosciences) containing fluorescein isothiocyanate–conjugated anti-human IFN-γ for 30 min at 4°C. Stained cells were analyzed using an EpicsXL flow cytometer (Beckman Coulter).

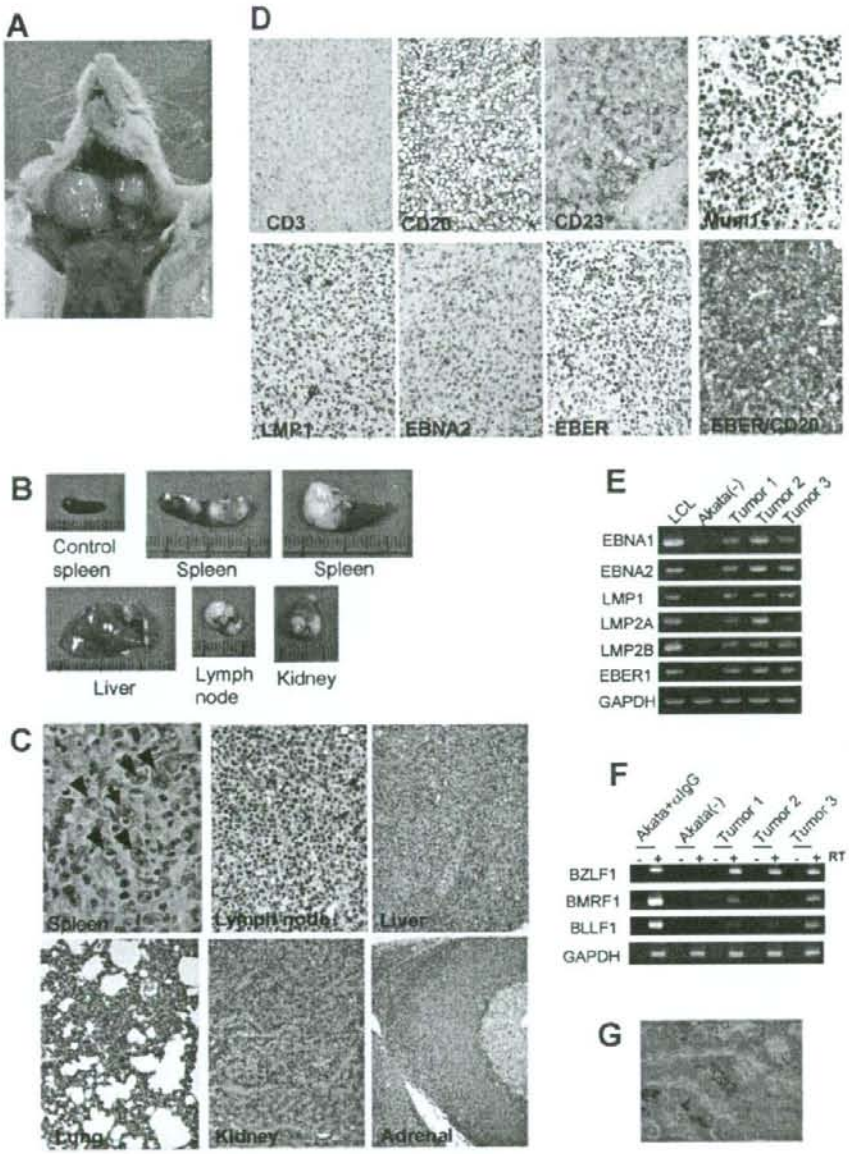

Figure 2. Pathological and virological analyses of Epstein-Barr virus (EBV)–infected humanized NOG (hNOG) mice. *A*, Photograph of an EBV-infected mouse showing tumors in the cervical area. *B*, Photographs of spleens, liver, lymph node, and kidney from EBV-infected mice with lymphoproliferative disorder. The upper left panel shows the spleen from an uninfected mouse. *C*, Photomicrographs of hematoxylin-eosin–stained tissues from mice with lymphoproliferative disorder. The arrow indicates a Reed-Sternberg–like cell, and the arrowheads indicate Hodgkin-like cells. Original magnifications, ×1000 for spleen, ×400 for lymph node, and ×200 for liver, lung, kidney, and adrenal gland. *D*, Immunohistochemical staining for lymphocyte surface markers (CD3, CD20, CD23, and Mum1) and EBV-encoded proteins (latent membrane protein [LMP] 1 and Epstein-Barr nuclear antigen [EBNA] 2), as well as in situ hybridization for EBV-encoded small RNA (EBER), in a lymph node from a mouse with lymphoproliferative disorder. The bottom right panel represents double staining for EBER and CD20. Original magnifications, ×200 for all except EBER/CD20, which is ×400. *E* and *F*, Reverse-transcription polymerase chain reaction detection of latent-cycle *(E)* and lytic-cycle *(F)* EBV gene expression in tumors from EBV-infected hNOG mice. Spleen tumors from 3 different mice were examined for the expression of EBNA1, EBNA2, LMP1, LMP2A, LMP2B, EBER1, BZLF1, BMRF1, and BLLF1. RNA samples from a lymphoblastoid cell line (LCL) *(E)* and anti-IgG–treated Akata cells *(F)* were used as positive controls, and an RNA sample from EBV-negative Akata cells (*E* and *F*) was used as a negative control. Assays were done with (+) or without (−) reverse transcriptase (RT) in panel F. Expression of GAPDH was examined as a reference. *G*, Double staining of EBER and CD20 in the liver of an hNOG mouse that was persistently infected with EBV without developing lymphoproliferative disorder. EBER is stained navy in the nucleus, and CD20 is stained brown in the membrane. Original magnification, ×1000.

Table 2. Quantification of Epstein-Barr virus (EBV) DNA in persistently infected humanized NOG mice.

Organ	Mouse	
	N35-1[a]	N35-3[b]
Bone marrow	ND	4.1×10^4
Spleen	6.2×10^2	5.7×10^3
Liver	ND	2.7×10^4
Lymph node (neck)	1.6×10^3	6.9×10^3
Lymph node (axilla)	ND	2.6×10^2
Lymph node (mesentery)	ND	4.1×10^2
Lungs	2.7×10^3	1.0×10^4
Kidneys	1.2×10^3	4.8×10^4
Adrenal gland	4.4×10^1	8.0×10^5

NOTE. Data are the amounts of EBV DNA measured 22 weeks after infection, in copies per microgram of DNA. ND, not detectable.

[a] Infected at 1×10^1 TD_{50}.

[b] Infected at 1×10^1 TD_{50}.

Detection of antibodies specific to EBV. IgM antibody to the EBV BFRF3 protein was detected by immunoblotting essentially as described elsewhere [24], except that horseradish peroxidase–conjugated antibody specific to human IgM (Beckman Coulter) was used as secondary antibody. To prepare the glutathione *s*-transferase (GST)–BFRF3 fusion protein, a DNA fragment spanning the entire coding region of BFRF3 was amplified by PCR (sense primer, 5'-GGCTCGAATTCATGGCACGCCGGCTGCCC-3'; antisense primer, 5'-GGCTCGGATCCATACACCATGTTTCGTGCCC-3') and inserted to the GST fusion vector pSGENT2, to yield the plasmid pSGENT2-BFRF3. *Escherichia coli* cells harboring pSGENT2-BFRF3 were stimulated with isopropyl β-D-1-thiogalactopyranoside to induce the expression of GST-BFRF3, which was subsequently purified by use of the Bulk GST Purification Module (GE Healthcare).

RESULTS

EBV infection in hNOG mice. Transplantation of human $CD34^+$ HSCs in NOG mice and reconstitution of the human hematoimmune system were done as described elsewhere [18, 20]. In the initial attempts at infection, 1×10^1 TD_{50} of the Akata strain of EBV was inoculated into 6 hNOG mice, and EBV DNA was demonstrated in the peripheral blood of all of them (figure 1*A*). EBV DNA was first evident at 3–4 weeks after inoculation and reached peak levels of $\sim 1 \times 10^6$ EBV DNA copies/μg of DNA. All 6 mice became seriously ill between 5 and 10 weeks after inoculation, with signs of weight loss (figure 1*A*), general inactivity, and piloerection. In contrast, EBV DNA was not detected in the peripheral blood, bone marrow, thymus, spleen, lymph nodes, liver, kidneys, and lungs of 3 control NOG mice that were not transplanted with HSCs but were inoculated with the virus (data not shown). Similarly, no signs of EBV infection were observed in 3 control hNOG mice that were not inoculated with the virus (data not shown). In total, 43 NOG mice that had been humanized with HSCs from 9 different cord blood samples were inoculated with 1×10^1 TD_{50} of EBV, and in 38 of them the results were similar to those observed in the initial 6 mice, with high blood EBV load and severe deterioration in their general condition. Ten of them died and could not be examined further. The remaining 28 mice were killed, and signs of lymphoproliferative disorder were found at autopsy (see the below). These results demonstrate that hNOG mice can be infected with EBV, with a mostly fatal outcome at this virus dose.

EBV-induced lymphoproliferative disorder in hNOG mice. Autopsy of killed mice showed signs of lymphoproliferative disorder typically represented by an overt tumor in the spleen (figure 2*B*). In ~70% (20/28) of the mice autopsied, macroscopical signs of disseminated disease were found in the liver, lymph nodes, or kidneys (figure 2*A* and 2*B*). Seventeen mice were examined pathologically, and 15 of them showed typical histology of diffuse large B cell lymphoma, with remarkable similarity to the human lymphoproliferative disorder in the immunocompromised hosts (figure 2*C*). The tissues contained occasional immunoblasts, Reed-Sternberg–like cells, and Hodgkin-like cells (figure 2*C*). Marked infiltration of large transformed lymphoid cells was also demonstrated in liver, lymph nodes, kidneys, adrenal glands, and lungs (figure 2*C*). Real-time PCR detected high levels ($\sim 1 \times 10^5$ to $\sim 1 \times 10^6$ EBV DNA copies/μg of DNA) of EBV DNA in these organs, and the large transformed lymphoid cells were universally EBV positive by EBER ISH (figure 2*D*). Immunohistochemical analysis showed that the large transformed lymphoid cells were of the activated B cell phenotype, being reactive for CD20 and CD23 and not reactive for CD3 and CD10 (figure 2*D* and data not shown). They were also positive for Mum-1, a late- and postgerminal center cell marker. The EBER-positive cells were CD20-positive B cells (figure 2*D*), and no EBER-positive T cells were identified. Immunostaining revealed that most proliferating cells expressed EBNA2, whereas LMP1 was expressed in only a fraction of them (figure 2*D*). RT-PCR analysis of typical spleen tumors obtained from 3 different mice showed the expression of EBNA1, EBNA2, LMP1, LMP2A, LMP2B; and EBER, consistent with the latency III program of EBV gene expression (figure 2*E*). In addition, transcripts from lytic-cycle EBV genes, including BZLF1 (immediate-early), BMRF1 (early), and BLLF1 (late, encoding gp350/220), were identified (figure 2*F*).

Virus dose–dependent outcome of EBV infection in hNOG mice. To examine the influence of virus dose on the outcome of EBV infection, we inoculated serial dilutions of EBV preparation into 2 lots of hNOG mice, each consisting of 5 mice that had been humanized with the same HSC preparation. Consistent with the results described above, the 4 mice (2 from each lot) that received the higher doses (1×10^3 and 1×10^2 TD_{50}) of the

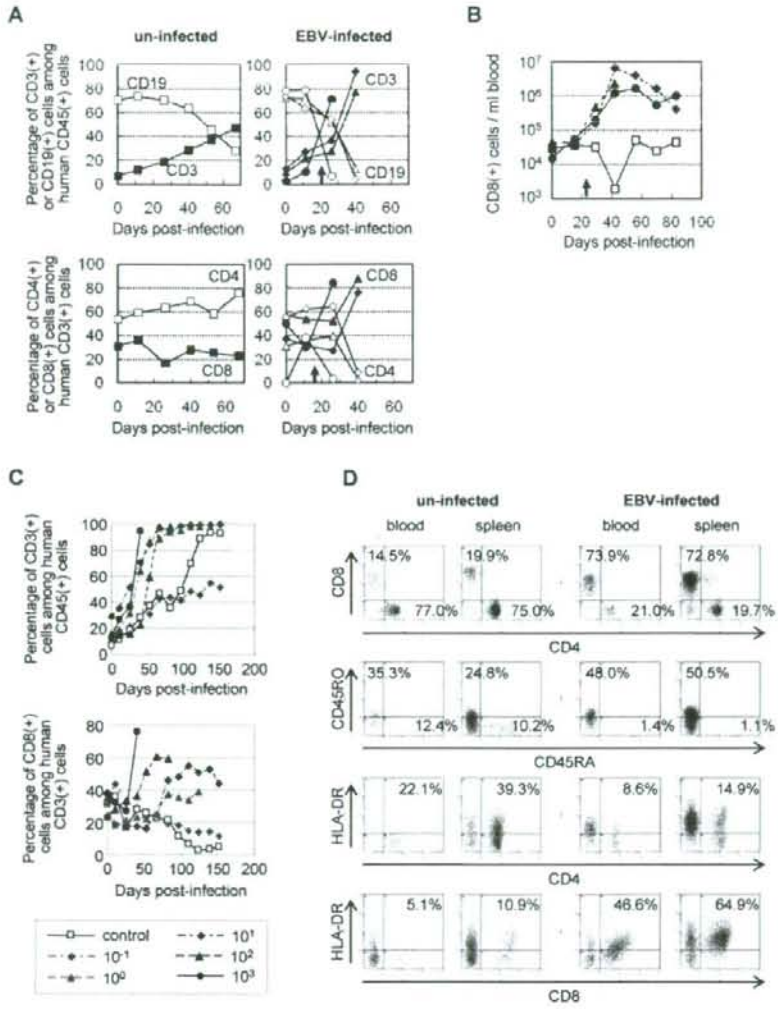

Figure 3. Surface marker expression by peripheral blood T cells in Epstein-Barr virus (EBV)–infected humanized NOG (hNOG) mice. *A*, Changes in the percentages of $CD3^+$ T cells and $CD19^+$ B cells among human $CD45^+$ leukocytes *(upper panels)* and in the percentages of $CD8^+$ cells and $CD4^+$ cells among $CD3^+$ cells *(lower panels)* after infection with EBV. Results obtained from 3 EBV-infected mice and an uninfected mice are shown. White symbols indicate the percentage of $CD19^+$ cells *(upper panels)* or $CD4^+$ cells *(lower panels)*; black symbols indicate the percentage of $CD3^+$ cells *(upper panels)* or $CD8^+$ cells *(lower panels)*. A vertical arrow in the graph area shows the time point at which EBV DNA was first detected in peripheral blood. *B*, Changes in the no. of $CD8^+$ T cells in the peripheral blood of EBV-infected hNOG mice. White symbols indicate uninfected mice, and black symbols indicate infected mice. Note that cell no. is plotted in a logarithmic scale. *C*, Viral dose–dependent T cell responses in hNOG mice inoculated with serially diluted EBV. Ten-fold serial dilutions of an EBV sample starting from 1×10^3 TD_{50} per inoculate were injected intravenously into NOG mice that had undergone transplantation with the same lot of human hematopoietic stem cells (HSCs). Changes in the percentages of $CD3^+$ T cells among human $CD45^+$ leukocytes *(upper panel)* and in the percentages of $CD8^+$ cells among $CD3^+$ cells *(lower panel)* after inoculation with EBV are shown. The viral dose for each mouse is shown in the key. *D*, Comparison of surface marker expression between EBV-infected mice and control mice. Two mice that underwent transplantation with the same lot of human HSCs were either inoculated with EBV or left uninfected; 10 weeks after inoculation, mononuclear cells obtained from peripheral blood or spleen were gated for the expression of human CD3 and then examined for the expression of CD8 and CD4 *(top panels)*, CD45RO and CD45RA *(second from top)*, HLA-DR and CD4 *(second from bottom)*, and HLA-DR and CD8 *(bottom)*.

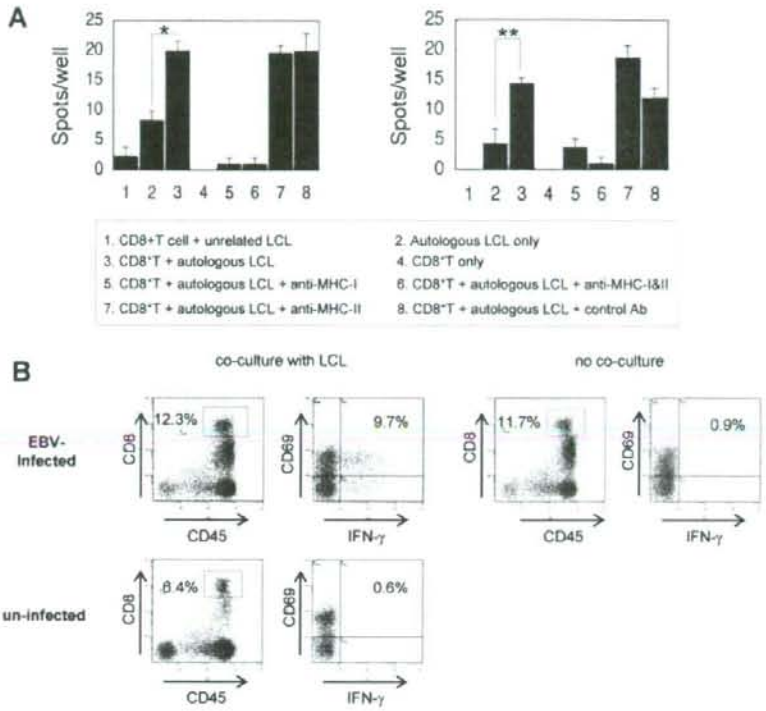

Figure 4. Epstein-Barr virus (EBV)–specific T cell response in humanized NOG (hNOG) mice. *A*, Enzyme-linked immunospot assay for the detection of human T cells producing interferon (IFN)–γ after stimulation with an EBV-positive lymphoblastoid cell line (LCL). $CD8^+$ cells isolated from EBV-infected hNOG mice were cocultured with an autologous LCL, and IFN-γ–secreting cells were counted (3, 5, 6, 7, and 8). To analyze restriction by major histocompatibility complex (MHC), antibody to HLA class I (anti–human HLA-ABC clone W6/32, eBioscience) (5), antibodies to both HLA class I and class II (6), antibody to HLA class II (anti–human HLA-DP,DQ,DR clone CR3/43; Dako) (7), or isotype-matched control antibody (8) were added to the culture. Control experiments included coculture of $CD8^+$ cells with an MHC-mismatched LCL (1), culture of the autologous LCL only (2), and culture of $CD8^+$ cells only (4). Results from 2 infected mice are shown. Five hundred $CD8^+$ cells per well were cultured in the experiment shown on the left, and 250 $CD8^+$ cells per well were cultured in that shown on the right. Spots were counted in triplicate in each of the 8 experimental groups, and the bars represent mean values and SEs. The unpaired Student's *t* test was used for statistical analysis. $^*P < .01$ and $^{**}P < .02$. *B*, Detection of human $CD8^+$ cells that produce IFN-γ in response to stimulation with an EBV-positive LCL by flow cytometry. $CD8^+$ cells were isolated from the spleen of an EBV-infected mouse and cocultured with the autologous LCL. Intracellular IFN-γ was stained and analyzed as described in Methods.

virus died of lymphoproliferative disorder ~5–10 weeks after inoculation. The remaining mice in both of the lots that received lower doses (1×10^1, 1×10^0, and 1×10^{-1} TD_{50}) survived acute infection and appeared normal throughout the observation period of 22 weeks. Although EBV DNA was detected at variable levels in their peripheral blood several weeks after inoculation, it returned to undetectable levels thereafter (figure 1*B*), suggesting that a certain protection mechanism worked to control EBV infection. Importantly, EBV DNA could be still detected in various organs, including spleen, liver, lungs, kidneys, and adrenal glands, at the end of the observation period (22 weeks), indicating that EBV persisted in these mice (table 2). Double staining for EBER and CD20 showed that EBV persisted in B cells (figure 2*G*). Macroscopical examination by autopsy at the end of the observation period did not reveal abnormality in these mice, except for moderate splenomegaly found in a mouse that received 1×10^1 TD_{50}. These results indicate that the outcome of EBV infection in hNOG mice varies with the virus dose; high doses of virus tend to cause fatal lymphoproliferative disorder, whereas lower doses induce apparently asymptomatic persistent infection.

EBV-specific T cell response in hNOG mice. Flow cytometry analysis demonstrated a dramatic increase in the percentage of $CD3^+$ T cells among the human $CD45^+$ leukocytes after infection with EBV. This increase in T cells was accompanied by an increase in the percentage of $CD8^+$ cells among human $CD3^+$ T cells. These changes were seen in virtually all infected mice, and the results from 3 mice are shown in figure 3*A*. The slow increase in the percentage of $CD3^+$ cells in the uninfected mouse represents the process of humanization (i.e., the development of hu-

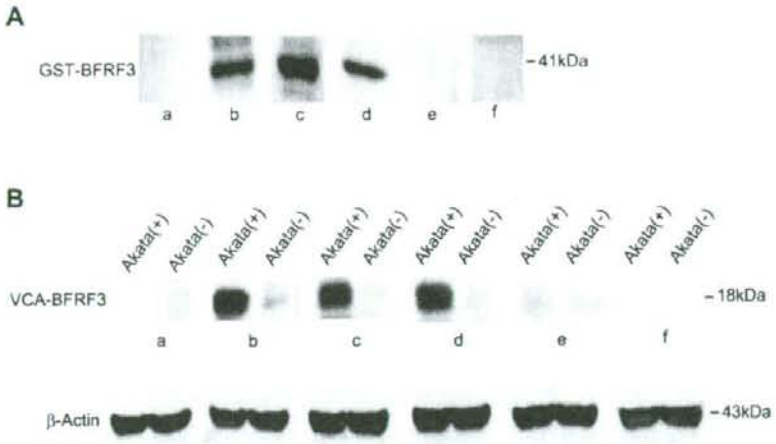

Figure 5. Demonstration of IgM antibody to the Epstein-Barr virus (EBV) BFRF3 protein in the serum of humanized NOG (hNOG) mice. *A*, Immunoblot with the glutathione *s*-transferase (GST)–BFRF3 fusion protein. Purified GST-BFRF3 fusion protein was examined with serum from an EBV-uninfected person *(a)*, an EBV-infected person *(b)*, EBV-infected hNOG mice (*c* and *d*), and an uninfected hNOG mice (*e* and *f*). *B*, Immunoblot with the lysate of EBV-producing Akata cells. Lysate of anti-IgG–treated Akata cells, labeled Akata(+), and of EBV-negative Akata cells, labeled Akata(−), was examined using serum from an EBV-uninfected person *(a)*, an EBV-infected person *(b)*, EBV-infected hNOG mice (*c* and *d*), and uninfected hNOG mice (*e* and *f*).

man T cells). This increase in $CD8^+$ cells were even more conspicuous when their definite number was counted (figure 3*B*). When hNOG mice were inoculated with serially diluted virus samples, a striking dose response was evident; mice inoculated with higher doses exhibited a more profound increase in $CD8^+$ cells at earlier time points (figure 3*C*). Further flow cytometry analyses showed that $CD45RO^+$ memory T cells, compared with $CD45RA^+$ T cells, increased in infected hNOG mice (figure 3*D*). Expression of a T cell activation marker, HLA-DR, was observed mainly in $CD8^+$ cells rather than in $CD4^+$ cells (figure 3*D*).

To demonstrate that these $CD8^+$ T cells were directed against EBV-infected cells, we examined IFN-γ secretion after stimulation with EBV-transformed cells. For this purpose, we first established an LCL using B cells isolated from the same cord blood that was used to isolate HSCs for transplantation. $CD8^+$ T cells, isolated from the peripheral blood of EBV-infected hNOG mice, were incubated with this autologous LCL, and cells secreting IFN-γ were detected by ELISPOT assay. For all 3 EBV-infected hNOG mice (which had been infected at 1×10^3 TD_{50}) thus examined, a significant number of spots were recognized in the wells in which $CD8^+$ T cells were mixed with the autologous LCL, whereas those cells incubated with unrelated LCL had many fewer spots (data from 2 mice are shown in figure 4*A*). $CD8^+$ T cells isolated from uninfected hNOG mice did not give a significant number of spots (data not shown). Release of IFN-γ was blocked by antibody specific to human major histocompatibility complex (MHC) class I but not by that specific to human MHC class II (figure 4*A*). These results clearly show that a T cell response restricted by human MHC class I was mounted against EBV-infected cells. In addition, in 5 of the 6 EBV-infected hNOG mice examined (infected at 1×10^3 TD_{50}), flow cytometry also demonstrated production of IFN-γ by $CD8^+$ T cells isolated from the spleen and stimulated with an autologous LCL (figure 4*B*).

EBV-specific antibody response in hNOG mice. Serum samples from 30 EBV-infected hNOG mice were examined by Western blotting for IgM antibodies reactive with a bacterially expressed GST-BFRF3 fusion protein. The BFRF3 protein is a major component of the virus capsid antigen of EBV [26]. The results are shown in figure 5*A* and indicated that four serum samples (from mice infected at 1×10^1 or 1×10^3 TD_{50}) contained IgM antibody reactive with it. These serum samples reacted also with the 18-kDa BFRF3-encoded protein in the lysate of Akata cells stimulated with IgG antibody to activate virus production (figure 5*B*). Similar experiments with human IgG–specific secondary antibody did not show a positive reaction with either GST-BFRF or $p18^{BFRF3}$. Six serum samples collected from uninfected hNOG mice reacted with neither the 18-kDa protein nor GST-BFRF3 (figure 5 and data not shown). These results indicate that hNOG mice have the ability to mount an IgM response to EBV.

DISCUSSION

The lymphoproliferative disease induced in hNOG mice is remarkably similar to the human lymphoproliferative disorder seen in immunocompromised hosts [27] with respect to histology, surface phenotype, and the type of EBV gene expression

(latency III). Reproduction of latency III in the present study makes for an interesting contrast with the previous model using NOD/*scid* mice, which exhibited the latency II pattern [10].

EBV infection in lower doses resulted in a transient increase in EBV DNA load in the peripheral blood, followed by apparently asymptomatic infection that persisted for at least 22 weeks. This type of asymptomatic EBV infection has not been described in nonprimate models of EBV infection and may be regarded as a model of human EBV latency. To compare this condition in NOG mice with EBV latency in humans precisely, we need to further investigate the nature of host cells (i.e., whether they are memory B cells), the pattern of EBV gene expression in them, and the involvement of anti-EBV immune responses in its maintenance.

In hNOG mice, human T cells develop in thymus tissue, in which epithelial cells are of murine origin [16]. It is therefore interesting that they could mount a T cell response restricted by human MHC class I. Although this suggests that positive selection of human T cells occurred in hNOG mice, the mechanism of T cell education remains unclear. Alloantigen-specific and human MHC class I–restricted T cell cytotoxicity has been reported in hNOG mice [15, 16]. An EBV-induced T cell response was evident in mice that received high doses of virus and developed lymphoproliferative disorder, suggesting that the T cell response in hNOG mice was not sufficient to control EBV-induced lymphoproliferation when they were infected at high doses. That only a minor fraction of $CD8^+$ T cells appeared to be EBV specific, as evidenced by ELISPOT assay and flow cytometry, may explain this result, at least partially. A humoral immune response to EBV has not been documented in previous mouse models of EBV infection, and therefore the NOG mouse may provide a valuable tool to analyze the mechanism and the protective roles of antibody response in EBV infection. We have to date clearly identified only IgM antibody to the 18-kDa component of virus capsid antigen in a minor fraction (4/30) of infected mice. We are currently attempting to improve sensitivity and to see whether hNOG mice can mount a more efficient and divergent antibody response to the virus, possibly including the production of IgG antibodies. Because both the T cell–mediated and the humoral immune response are elicited in hNOG mice, they may be useful in the evaluation of candidate EBV vaccines.

Very recently, humanized mice based on other immunodeficient mouse strains were prepared, and EBV was used as a typical pathogen to analyze their immune functions. Traggiai et al. [12] infected humanized $Rag2^{-/-}$IL-$2R\gamma^{-/-}$ mice with EBV and documented an in vitro proliferative response by $CD8^+$ T cells to an autologous LCL. Melkus et al. [11], on the other hand, humanized NOD/*scid* mice by transplanting human fetal liver, thymus, and HSCs and succeeded in inducing an EBV-specific T cell immune response as well as an innate immune response to toxic shock syndrome toxin 1. These 2 studies were performed mainly using immunological standpoints and did not provide detailed data from virological investigations. An advantage of the NOG mouse model described here is that it does not require a fine surgical procedure using human fetal tissue; therefore, NOG mice can be easily provided in large quantities.

In immunocompromised humans, failure of immunosurveillance may lead to the development of lymphoproliferative disorder. We expect that the NOG mouse model can be used to analyze the exact relationship between immunodeficiency and the development of lymphoproliferative disorder. Immune responses in the hNOG mouse can be modulated by immunosuppressive drugs (such as cyclosporine A) or HIV, and the development of lymphoproliferative disorder can be analyzed with special reference to the nature and level of immunodeficiency. This kind of study, which has not been possible with conventional *scid* mice, may reveal an exact condition in which lymphoproliferative disorder develops and may thereby aid the development of a specified immunosuppressive procedure that evades this condition and precludes the risk of lymphoproliferative disorder.

In summary, the NOG mouse is able to recapitulate various essential elements of human EBV infection and is therefore, to our knowledge, the most comprehensive small-animal model of EBV infection described to date. It should be a valuable tool for the study of the pathogenesis, prevention, and treatment of EBV infection.

Acknowledgments

We thank Satoshi Itakura, Fuyuko Kawano, Eri Yamada, Miki Mizukami, and Ken Watanabe for technical assistance. We thank Shizuko Minegishi for advice on flow cytometry, Atsushi Komano for advise on the enzyme-linked immunospot assay, Ayako Demachi-Okamura and Kiyotaka Kuzushima for advice on detection of Epstein-Barr virus–specific T cells, and Shosuke Imai for helpful discussions. We thank the Tokyo Cord Blood Bank for supplying cord blood.

References

1. Rickinson AB, Kieff E. Epstein-Barr virus. In: Knipe DM, Howley PM, eds. Fields virology. Philadelphia: Lippincott Williams & Wilkins, **2001**: 2575–628.
2. Kieff E, Rickinson AB. Epstein-Barr virus and its replication. In: Knipe DM, Howley PM, eds. Fields virology. 4th ed. Philadelphia: Lippincot Williams & Wilkins, **2001**:2511–74.
3. Young LS, Finerty S, Brooks L, Scullion F, Rickinson AB, Morgan AJ. Epstein-Barr virus gene expression in malignant lymphomas induced by experimental virus infection of cottontop tamarins. J Virol **1989**; 63: 1967–74.
4. Miller G, Shope T, Coope D, et al. Lymphoma in cotton-top marmosets after inoculation with Epstein-Barr virus: tumor incidence, histologic spectrum antibody responses, demonstration of viral DNA, and characterization of viruses. J Exp Med **1977**; 145:948–67.
5. Cho Y, Ramer J, Rivailler P, et al. An Epstein-Barr-related herpesvirus from marmoset lymphomas. Proc Natl Acad Sci USA **2001**; 98:1224–9.
6. Moghaddam A, Rosenzweig M, Lee-Parritz D, Annis B, Johnson RP, Wang F. An animal model for acute and persistent Epstein-Barr virus infection. Science **1997**; 276:2030–3.
7. Mosier DE, Gulizia RJ, Baird SM, Wilson DB. Transfer of a functional human immune system to mice with severe combined immunodeficiency. Nature **1988**; 335:256–9.

8. Okano M, Taguchi Y, Nakamine H, et al. Characterization of Epstein-Barr virus-induced lymphoproliferation derived from human peripheral blood mononuclear cells transferred to severe combined immunodeficient mice. Am J Pathol **1990**; 137:517–22.
9. Rowe M, Young LS, Crocker J, Stokes H, Henderson S, Rickinson AB. Epstein-Barr virus (EBV)-associated lymphoproliferative disease in the SCID mouse model: implications for the pathogenesis of EBV-positive lymphomas in man. J Exp Med **1991**; 173:147–58.
10. Islas-Ohlmayer M, Padgett-Thomas A, Domiati-Saad R, et al. Experimental infection of NOD/SCID mice reconstituted with human CD34+ cells with Epstein-Barr virus. J Virol **2004**; 78:13891–900.
11. Melkus MW, Estes JD, Padgett-Thomas A, et al. Humanized mice mount specific adaptive and innate immune responses to EBV and TSST-1. Nat Med **2006**; 12:1316–22.
12. Traggiai E, Chicha L, Mazzucchelli L, et al. Development of a human adaptive immune system in cord blood cell-transplanted mice. Science **2004**; 304:104–7.
13. Hiramatsu H, Nishikomori R, Heike T, et al. Complete reconstitution of human lymphocytes from cord blood CD34+ cells using the NOD/SCID/γ_c^{null} mice model. Blood **2003**; 102:873–80.
14. Ito M, Hiramatsu H, Kobayashi K, et al. NOD/SCID/γ_c^{null} mouse: an excellent recipient mouse model for engraftment of human cells. Blood **2002**; 100:3175–82.
15. Yahata T, Ando K, Nakamura Y, et al. Functional human T lymphocyte development from cord blood CD34+ cells in nonobese diabetic/Shi-scid, IL-2 receptor gamma null mice. J Immunol **2002**; 169:204–9.
16. Ishikawa F, Yasukawa M, Lyons B, et al. Development of functional human blood and immune systems in NOD/SCID/IL2 receptor γ chain^{null} mice. Blood **2005**; 106:1565–73.
17. Miyazato P, Yasunaga J, Taniguchi Y, Koyanagi Y, Mitsuya H, Matsuoka M. De novo human T-cell leukemia virus type 1 infection of human lymphocytes in NOD-SCID, common gamma-chain knockout mice. J Virol **2006**; 80:10683–91.
18. Watanabe S, Terashima K, Ohta S, et al. Hematopoietic stem cell-engrafted NOD/SCID/IL2Rgamma null mice develop human lymphoid systems and induce long-lasting HIV-1 infection with specific humoral immune responses. Blood **2007**; 109:212–8.
19. Dewan MZ, Terashima K, Taruishi M, et al. Rapid tumor formation of human T-cell leukemia virus type 1-infected cell lines in novel NOD-SCID/gammac^{null} mice: suppression by an inhibitor against NF-kappaB. J Virol **2003**; 77:5286–94.
20. Watanabe S, Ohta S, Yajima M, et al. Humanized NOD/SCID/IL2Rγ^{null} mice transplanted with hematopoietic stem cells under nonmyeloablative conditions show prolonged life spans and allow detailed analysis of human immunodeficiency virus type 1 pathogenesis. J Virol **2007**; 81: 13259–64.
21. Takada K, Ono Y. Synchronous and sequential activation of latently infected Epstein-Barr virus genomes. J Virol **1989**; 63:445–9.
22. Condit RC. Principles of virology. In: Knipe DM, Howley PM, eds. Fields virology. Philadelphia: Lippincott Williams & Wilkins. **2001**:19–51.
23. Kimura H, Morita M, Yabuta Y, et al. Quantitative analysis of Epstein-Barr virus load by using a real-time PCR assay. J Clin Microbiol **1999**; 37:132–6.
24. Nakamura H, Iwakiri D, Ono Y, Fujiwara S. Epstein-Barr-virus-infected human T-cell line with a unique pattern of viral-gene expression. Int J Cancer **1998**; 76:587–94.
25. Kuzushima K, Hoshino Y, Fujii K, et al. Rapid determination of Epstein-Barr virus-specific CD8$^+$ T-cell frequencies by flow cytometry. Blood **1999**; 94:3094–100.
26. van Grunsven WM, Nabbe A, Middeldorp JM. Identification and molecular characterization of two diagnostically relevant marker proteins of the Epstein-Barr virus capsid antigen complex. J Med Virol **1993**; 40: 161–9.
27. Rezk SA, Weiss LM. Epstein-Barr virus-associated lymphoproliferative disorders. Hum Pathol **2007**; 38:1293–304.

THE JOURNAL OF BIOLOGICAL CHEMISTRY VOL. 283, NO. 44, pp. 30045–30056, October 31, 2008
© 2008 by The American Society for Biochemistry and Molecular Biology, Inc. Printed in the U.S.A.

AML1/RUNX1 Works as a Negative Regulator of c-Mpl in Hematopoietic Stem Cells*

Received for publication, June 23, 2008, and in revised form, August 6, 2008 Published, JBC Papers in Press, August 7, 2008, DOI 10.1074/jbc.M804768200

Yusuke Satoh[‡], Itaru Matsumura[‡1], Hirokazu Tanaka[‡], Sachiko Ezoe[‡], Kentaro Fukushima[‡], Masahiro Tokunaga[‡], Masato Yasumi[‡], Hirohiko Shibayama[‡], Masao Mizuki[‡], Takumi Era[§], Tsukasa Okuda[¶], and Yuzuru Kanakura[‡]

From the [‡]Department of Hematology and Oncology, Osaka University Graduate School of Medicine, 2-2 Yamada-oka, Suita, Osaka 565-0871, the [§]Division of Molecular Neurobiology, Institute of Molecular Embryology and Genetics, Kumamoto University, Kumamoto 860-0811, and the [¶]Department of Biochemistry and Molecular Biology, Kyoto Prefectural University of Medicine, Kyoto 602-8566, Japan

In this study, we analyzed the roles for AML1/RUNX1 in the regulation of the c-*mpl* promoter. Wild-type AML1 activated the c-*mpl* promoter through the proximal AML-binding site in luciferase assays using 293T and HeLa cells. In accord with this result, electrophoretic mobility shift assay and chromatin immunoprecipitation assays demonstrated that AML1 bound to this site. Next, we analyzed the function of AML1 using a mutant of AML1 lacking the C terminus (AML1dC), which was originally found in a patient with myelodysplastic syndromes. AML1dC dominant-negatively suppressed transcriptional activity of wild-type AML1. However, unexpectedly, AML1dC-transduced murine c-Kit$^+$Sca1$^+$Lineage$^-$ cells expressed c-*mpl* mRNA and c-Mpl protein more abundantly than mock-transduced cells, which led to the enhanced thrombopoietin-mediated proliferation. Moreover, when AML1dC was induced to express during the development of hematopoietic cells from embryonic stem (ES) cells, AML1dC augmented the c-Mpl expression on hematopoietic stem/progenitor cells. Furthermore, we found that early hematopoietic cells that derived from AML1$^{+/-}$ ES cells expressed c-Mpl more intensely than those that developed from wild-type ES cells. In contrast, AML1dC hardly affected c-Mpl expression and maturation of megakaryocytes. As for the mechanism of the different roles of AML1 in the regulation of the c-*mpl* promoter, we found that AML1 forms a complex with a transcription repressor mSin3A on the c-*mpl* promoter in hematopoietic stem/progenitor cells, although it forms a complex with a transcription activator p300 on the same promoter in megakaryocytic cells. Together, these data indicate that AML1 can regulate the c-*mpl* promoter both positively and negatively by changing the binding partner according to cell types.

AML1 (RUNX1) is a family member of heterodimeric transcription factors named core binding factors. *AML1* was originally identified at a breakpoint on human chromosome 21 in the t(8;21) translocation and known as the most common targets of chromosomal translocations in human leukemia (1, 2). In addition to chromosomal translocations, recent reports have shown the importance of point mutations of AML1 in hematological malignancies, such as acute myelogenous leukemia (AML)[2] and myelodysplastic syndromes (MDS) (3). The Runt domain of AML1 is utilized for DNA binding and heterodimerization with a partner PEBP2β/CBFβ. Although PEBP2β by itself does not bind to the DNA, the association with PEBP2β is necessary for AML1 to elicit its biologic activity (4–6). AML1 can regulate the transcription of the target gene both positively and negatively through the binding to the consensus DNA sequence, TGT/cGGT, possibly dependent on the cellular context and/or its target gene. For example, it positively regulates the expression cytokines and their receptors in myeloid and lymphoid lineage cells (7–12), whereas it negatively regulates CD4 transcription in immature thymocytes (13). Several experiments using conventional and conditional gene targeting in mice demonstrated that AML1 is essential for the early step in definitive hematopoiesis (14). North *et al.* (15) revealed that AML1 is required for the generation of hematopoietic stem cells (HSCs) from the vitelline and umbilical arteries and from the aorta-gonad-mesonephros (AGM) region. In addition, AML1 is necessary for the transitions from the stage of double-negative (DN)2 to DN3 and DN3 to DN4 in the T-lymphocyte development (9, 17). Furthermore, AML1 plays an important role in the maturation of megakaryocytes and platelet production. AML1 deletion in adult mice led to the impaired polyploidization of megakaryocytes and low platelet production (17, 18), whereas the number of megakaryocyte progenitors was not altered in these mice, suggesting that AML1 is indispensable for the terminal maturation of megakaryocytes. Also, the hereditary loss-of-function mutation of AML1 or

* This work was supported by grants from the Ministry of Education, Science, Sports, and Culture and Technology of Japan and the Sankyo Foundation of Life Science. The costs of publication of this article were defrayed in part by the payment of page charges. This article must therefore be hereby marked "*advertisement*" in accordance with 18 U.S.C. Section 1734 solely to indicate this fact.

[1] To whom correspondence should be addressed. Tel.: 81-6-6879-3871; Fax: 81-6-6879-3879; E-mail: matumura@bldon.med.osaka-u.ac.jp.

[2] The abbreviations used are: AML, acute myelogenous leukemia; HSC, hematopoietic stem cells; EMSA, electrophoretic mobility shift assay; ES, embryonic stem cell; TPO, thrombopoietin; ChIP, chromatin immunoprecipitation; FACS, fluorescence-activated cell sorter; DMEM, Dulbecco's modified Eagle's medium; FBS, fetal bovine serum; Ab, antibody; MDS, myelodysplastic syndrome; FITC, fluorescein isothiocyanate; CLP, common lymphoid progenitor; GFP, green fluorescent protein; RT, reverse transcription; DN, double-negative; h, human; m, murine; IL, interleukin; WT, wild type; MT, mutant; Tet, tetracycline; SCF, stem cell factor; BFU-E, burst-forming unit-erythroid; CFU-GM, colony-forming unit-granulocyte macrophage; CFU-GEMM, colony-forming unit-granulocyte erythrocyte monocyte macrophage.

Downloaded from www.jbc.org at OSAKA UNIVERSITY on February 1, 2009

PEBP2β causes familial platelet disorder with predisposition to AML (FPD/AML), which is characterized by decreased platelet count and propensity to develop AML (19).

MDS are clonal hematological disorders derived from gene alteration at a level of HSC (20), which are characterized by ineffective hematopoiesis, dysplastic morphology of blood cells, and high possibility to transit to AML. A number of genetic or epigenetic alterations involved in the pathogenesis of MDS have been identified as follows: activating point mutations of signaling molecules such as N-RAS and Flt3 (21, 22); deletion, point mutation, and/or silencing of cell cycle inhibitory molecules such as p15, p16, and p53 (23–25); deletion, point mutation, and generation of chimeric genes for transcriptional factors such as Evi1, IRF-1, AML1 (26–28), and point mutations of the nucleolar protein (Nucleophosmin) (29). Among them, the point mutations of *AML1* were found in 15–17% of patients with sporadic MDS/AML (high risk MDS and AML following MDS) (3, 30). Previously, point mutations of AML1 were intensively screened in the N-terminal region, including the Runt domain in patients with AML and MDS, and the researchers found several point mutations, most of which disrupts DNA binding activity of AML1 but not the interaction with PEBP2β (3). In addition, recent reports have revealed that about 50% of point mutations are detected in the C-terminal region in MDS/AML. In addition, a C-terminal *AML1* point mutation was also detected FPD/AML (30, 31). Most of the C-terminal mutations of AML1 lead to the premature termination yielding the C-terminally truncated form of AML1, which inhibits transcriptional activity of AML1.

Thrombopoietin (TPO) is a crucial regulator of megakaryopoiesis and platelet production. It stimulates both megakaryocyte progenitor cell growth and subsequent maturation *in vitro* and *in vivo* (32). In accord with these data, knock-out mice for TPO or its receptor c-*mpl* both revealed severely impaired megakaryopoiesis and platelet reduction (about 5% of normal mice) without apparent abnormality in erythropoiesis, granulopoiesis, and lymphopoiesis, suggesting that a physiologic role of the TPO/c-Mpl system is restricted to the megakaryocytic lineage. However, in the later study, the total number of HSCs was found to be reduced in the bone marrow of c-Mpl$^{-/-}$ mice (57). Also, c-Mpl$^{-/-}$ HSCs revealed severely decreased reconstitution activity in transplantation experiments. These results indicate that TPO/c-Mpl-mediated signaling also plays an important role in the growth and survival of HSCs as well as in megakaryopoiesis (33, 34).

Considering the fact that both AML1 and TPO/c-Mpl signaling play crucial roles in the growth and survival of HSCs as well as in megakaryopoiesis, we speculate the transcriptional regulation by AML1 might have some influence on TPO/c-Mpl signaling. So, we here examined the effects of AML1 on the c-Mpl transcription using the promoter analyses. Also, we analyzed the biologic effects of AML1dC on c-Mpl expression in HSC and megakaryocytes and on megakaryocytic differentiation.

EXPERIMENTAL PROCEDURES

Reagents and Antibodies—Recombinant human (h) interleukin-6 (hIL-6), murine (m) IL-3, murine stem cell factor (mSCF), human thrombopoietin (hTPO), human erythropoietin, and an anti-mouse c-Mpl monoclonal antibody were provided by Kirin Brewery Co. (Tokyo, Japan). Human flt3-ligand was purchased from PeproTech (London, UK). Fluorescein isothiocyanate (FITC)-conjugated rat IgG1 and biotinylated rat IgG2b were purchased from Immunotech (Marseilles, France). Biotinylated anti-lineage (Lin) antibodies (Abs) against Gr-1 (RB6-8C5), B220 (RA3-6B2), CD3 (145-2C11), Mac1 (M1/70), and Ter119 (TER119), FITC-labeled anti-Sca-1(D7), phycoerythrin-labeled anti-c-Kit (2B8), phycoerythrin-conjugated anti-Rat Igλ (B46-5), and streptavidin-PerCP-Cy5.5 were purchased from BD Biosciences. The anti-AML-1 Ab (N-20) and normal goat IgG were purchased from Santa Cruz Biotechnology (Santa Cruz, CA).

Plasmid Constructs—The expression vectors for AML1b and AML1-MTG8 (pRCCMV-AML1b and pRCCMV-AML1-MTG8) were kindly provided by Dr. Kitabatashi (National Cancer Center Research Institute, Tokyo, Japan) (35). AML1dC, lacking the C terminus of AML1b (amino acids from 224 to 453), was obtained by the PCR method. Retrovirus expression vectors for AML1b and AML1dC were generated by subcloning these cDNAs into the Mie vector (pMSCV-IRES-EGFP). The expression vector for PEBP2β was provided by Dr. N. A. Speck (Dartmouth Medical School, Hanover, NH) (36).

Luciferase Assays—To construct reporter genes for the c-*mpl* promoter, various PCR products were subcloned into the luciferase plasmid, PSP72-Luc (37). Luciferase assays were performed with a dual luciferase reporter system (Promega, Madison, WI) as described previously (37). In short, 293T cells (2×10^5 cells) cultured in DMEM containing 10% fetal bovine serum (FBS) were seeded into a 60-mm dish and transfected with the effector genes (2 μg) and reporter gene (2 μg) together with pRL-CMV-Rluc (5 ng), an expression vector for *Renilla* luciferase, by the calcium phosphate coprecipitation method. After 12 h, the cells were washed and serum-deprived for 24 h. Then the cells were lysed and subjected to the measurement of the firefly and *Renilla* luciferase activities on a luminometer LB96P (Berthold Japan, Tokyo, Japan). The relative firefly luciferase activities were calculated by normalizing transfection efficiencies according to the *Renilla* luciferase activities. To perform luciferase assays in HeLa cells, we used a FuGENE 6 (Roche Applied Science) for transfection. The experiments were performed in triplicate, and the similar results were obtained from at least three independent experiments.

Electrophoretic Mobility Shift Assay (EMSA)—EMSA was performed as described previously (38). One probe used as a positive control contained the reported AML1-binding sequence (39). One more probe contained the proximal putative AML1-binding sequence in the human c-*mpl* promoter (−135/−116, numbered from the first ATG). For competition assays, unlabeled oligonucleotides containing wild-type (WT) (TGTGGT) or mutated (MT) (TGTTAG) AML1-binding site were added to the DNA-binding reaction mixtures. The sequences of the oligonucleotides are as follows: WT AML1, 5′-CGAGTATTGTGGTTAATACG-3′; MT AML1, 5′-CGAGTATTGTTAGTAATACG-3′; c-*mpl* (−135/−116) WT, 5′-ACCCCAGTGTGGTCTGGATG-3′; and c-*mpl* (−135/−116) MT, 5′-ACCCCAGTGTTAGCTGGATG-3′.

Downloaded from www.jbc.org at OSAKA UNIVERSITY on February 1, 2009

Chromatin Immunoprecipitation (ChIP) and ReChIP Assays—ChIP assays were performed with a ChIP assay kit (Upstate Biotechnology Inc.). Briefly, 1×10^7 cells were fixed with 1% formaldehyde for 10 min. Cross-links were quenched with 125 mM glycine. After isolation of the nuclear extract, chromatin was sonicated to shear DNA to the length between 200 and 1000 bp. After sonication, AML1-DNA-binding complexes were immunoprecipitated with the anti-AML1 Ab or control goat IgG. The immunoprecipitated DNA was eluted and subjected to the PCRs using AmpliTaq Gold (PerkinElmer Life Sciences), in the following thermal cycling conditions: 94 °C for 10 min, 30 cycles of 94 °C for 30 s, 65 °C for 30 s, and 72 °C for 30 s, followed by 72 °C for 10 min. The sequences of the primer set for the human c-*mpl* promoter are as follows: sense, 5′-TTTCCCCAGTGTGGTCTGGATGG-3′; antisense, 5′-TTTGCCTTAGCCCATCCTCCCTT-3′. PCR products were electrophoresed on agarose gels and visualized by staining with SYBR Green I (BioWhittaker Molecular Applications, Rockland, ME). In the sequential ChIP (ReChIP) experiments, we performed a first ChIP with the anti-AML1 Ab. Immunoprecipitated complexes were eluted by incubation for 30 min at 37 °C in 50 μl of 10 mmol/liter dithiothreitol. After centrifugation, the supernatant was diluted 20 times with ReChIP buffer (1% Triton X-100, 2 mmol/liter EDTA, 150 mmol/liter NaCl, 20 mmol/liter Tris-HCl, (pH 8.0)) and subjected to the second re-immunoprecipitation and the ChIP procedure. In the ReChIP analysis, PCRs were performed with 35 cycles of amplification (40, 41).

Purification of Murine c-Kit$^+$ Sca1$^+$ Lin$^-$ (KSL) Cells—Bone marrow cells were harvested from 8- to 10-week-old C57BL/6 mice, and mononuclear cells were isolated by density gradient centrifugation. After staining with biotinylated anti-Lin Abs, an FITC-conjugated anti-Sca1 Ab, a phycoerythrin-conjugated anti-c-Kit A, and a streptavidin-PerCP-Cy5.5, KSL cells were sorted on FACS Aria (BD Biosciences).

Preparation of the Conditioned Medium Containing Retrovirus Particles—Conditioned medium containing high tighter retrovirus particles was prepared as reported previously (38). Briefly, retrovirus plasmid DNA was transfected into retrovirus packaging cell line 293gp along with a vesicular stomatitis virus-G envelope expression plasmid by the calcium phosphate coprecipitation method. After 48 h, cultured supernatant was collected and concentrated by 100-fold in volume.

Retrovirus Transfection into Murine Hematopoietic Stem/Progenitor Cells—Purified KSL cells were cultured in DMEM containing 10% FBS, mSCF (100 ng/ml), and hTPO (100 ng/ml). Then the cells were seeded into the culture plates coated with Retronectin (TAKARA BIO, Shiga, Japan) and cultured with conditioned medium containing retrovirus and Polybrene (10 μg/ml) in the presence of mSCF (100 ng/ml) and hTPO (100 ng/ml). After 24 h, cells were washed and cultured in DMEM containing 10% FBS, mSCF (50 ng/ml), human flt3-ligand (30 ng/ml), and hIL-6 (50 ng/ml).

Flow Cytometry—Two days after retrovirus infection, GFP$^+$ cells were sorted by FACS Aria (BD Biosciences). Cell surface marker analyses were performed with FACSCalibur (BD Biosciences). DNA content of cultured cells was examined by staining with propidium iodide and analyzed by the same device. FACS data were analyzed by FlowJo software (TreeStar, Ashland, OR). To analyze TPO-dependent tyrosine phosphorylation of STAT5, we used BD Phosflow™ Technology (BD Biosciences). Two days after retrovirus infection, Mock-, AML1dC-, and AML1b-transduced cells were cultured in DMEM containing 2% FBS without cytokines for 4 h. The cytokine-deprived cells were then stimulated with hTPO (100 ng/ml) for 15 min. Fixed samples were stained with Alexa Fluor®647 STAT5 (pY694) and analyzed by FACS Aria (BD Biosciences).

RT-PCR—For RT-PCR, total RNA was isolated from 7×10^3 GFP$^+$ cells and was reverse-transcribed into cDNA with oligo(dT) primers (Pharmacia, Piscataway, NJ) using SuperScript II reverse transcriptase (Invitrogen). PCR was performed in a total volume of 50 μl using 4 μl of the cDNA product as a template and 1 μl of Advantage cDNA polymerase mix (Clontech). The primer sets to amplify murine c-*mpl* and β-actin are as follows: c-*mpl*, 5′-CCTACTGCTGCTAAAGTGGCAAT-3′ and 5′-CAATAGCTTAGTGGTAGGTAGGA-3′; β-actin, 5′-CATCACTATTGGCAACGAGC-3′ and 5′-ACGCAGCTCAGTAACAGTCC-3′. Cycling conditions were 94 °C for 1 min, followed by 22–35 cycles of 94 °C for 30 s and 68 °C for 3 min, followed by 68 °C 5 min. The PCR products were electrophoresed on agarose gels, and their amounts were evaluated by staining with SYBR Green I (BioWhittaker Molecular Applications, Rockland, ME).

OP9 System to Develop Hematopoietic Cells from Murine ES Cells—E14tg2a ES cells and OP9 stromal cells were maintained as described previously (42, 43). To induce differentiation toward hematopoietic cells, ES cells were deprived of leukemia inhibitory factor and seeded onto confluent OP9 cells in 6-well plates at a density 10^4 cells/well in α-minimum essential medium supplemented with 20% FBS. After 4.5 days, Flk-1$^+$ cells were sorted by FACS or the cells were harvested by 0.25% trypsin/EDTA, and whole cell suspensions were transferred into a new 10-cm dish and incubated in 37 °C for 30 min to remove adherent OP9 cells. The collected floating cells were replated onto OP9 cells at a density 1×10^4 cells/well of 6-well plate or 6×10^4 cells/10-cm dish and cultured under the indicated conditions.

Tetracycline (Tet)-regulated Inducible Expression of AML1dC in ES Cells—To inducibly express AML1dC in ES cells, we utilized a Tet-Off system as reported previously (44, 45), in which transcription of the target mRNA is initiated by the removal of Tet from the culture medium. Briefly, we initially introduced pCAG20-1-tTA and pUHD10-3-puro by electroporation (800 V, 3 microfarads) and selected one clone designated E14 by the culture with 1 μg/ml of Puro and/or 1 μg/ml of Tet, in which the Tet-regulatory system works most effectively. We further transfected pUHD10–3-AML1dC-GFP, which can inducibly express AML1dC and GFP as a single mRNA through the internal ribosome entry site in response to the Tet removal, together with the neomycin-resistant plasmid pcDNA3.1-neo. After the culture with G418 (0.4 mg/ml) in the Tet$^+$ medium, we selected several clones that can inducibly express GFP in response to the Tet deprivation. Subsequently, we examined the Tet-regulated expression of AML1dC in the

Downloaded from www.jbc.org at OSAKA UNIVERSITY on February 1, 2009

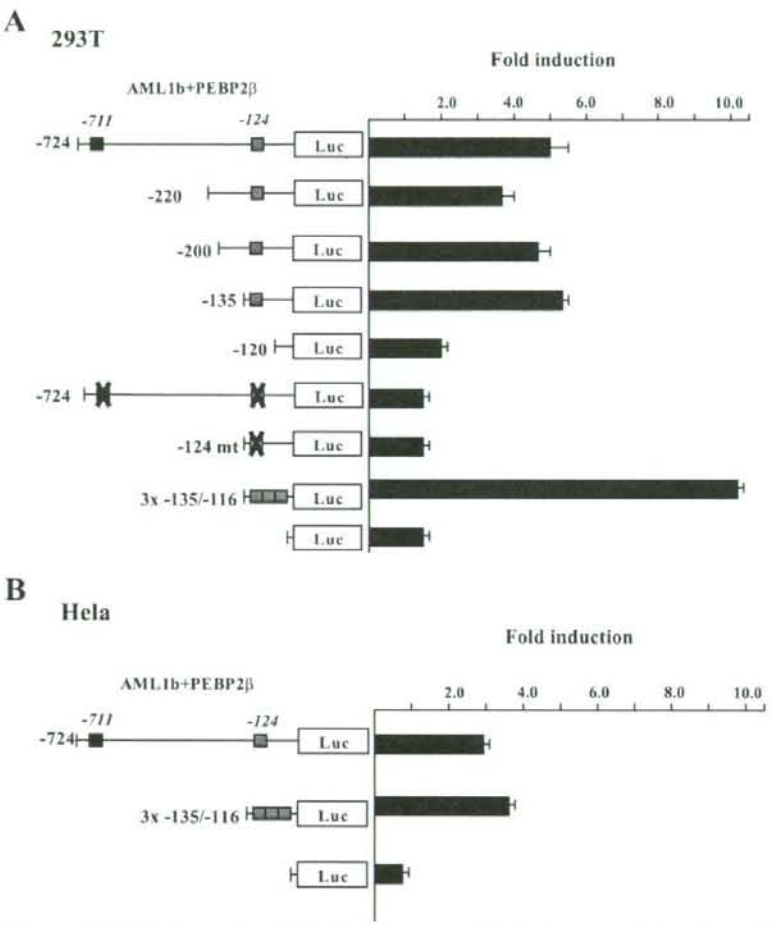

FIGURE 1. **Effects of AML1b on the activity of *c-mpl* promoter.** *A*, 293T cells were transfected with 2 μg of AML1b, PEBP2β, and 2 μg of indicated reporter gene. The relative firefly luciferase (*LUC*) activities were calculated by normalizing transfection efficiencies according to the *Renilla* luciferase activities. The results are shown as the means ± S.D. of triplicate cultures. *B*, HeLa cells were transfected with 0.5 μg of AML1b and PEBP2β and 1 μg of reporter genes by FuGENE 6.

proximal 724 bp of the c-*mpl* promoter using 293T cells. As shown in Fig. 1*A*, WT AML1b activated the −724 construct about 5.0-fold in the presence of its heterodimerization partner, PEBP2β. As there were two putative AML1-binding sites (TGTGGT) in the −724 construct, we further constructed several deletion mutants. Although deletion of the distal AML1-binding site (−711) and extended deletion up to −135 bp did not influence the c-*mpl* promoter activation by AML1b, the −120 construct further lacking the proximal AML1-binding site (−124) was scarcely activated by AML1. In addition, AML1b could not activate −124mt construct, in which the proximal AML1-binding site was changed from TGTGGT to TGTTAG. Furthermore, AML1 activated the 3× −135/−116 construct containing three tandem repeats of the proximal AML1-binding site and minimal JunB promoter over 10-fold. Similar results were obtained from luciferase assays using HeLa cells (Fig. 1*B*). These results suggest that AML1 may regulate the expression of c-*mpl* through the proximal AML1-binding site in the promoter.

AML1 Transcriptionally Regulates the c-mpl Promoter—To analyze whether AML1 directly binds to the proximal AML1-binding sequence in the c-*mpl* promoter, we performed EMSA with the corresponding c-*mpl* (−135/−116) probe. Also, one more probe with the reported AML1-binding sequence (39, 46) was used as a positive control. Nuclear extracts were isolated from 293T cells that were transfected with PEBP2β with or without AML1b. As compared with the nuclear extract from AML1b-untransfected 293T cells (Fig. 2*A*, *lane 1*), that from AML1b-transfected cells formed two additional complexes with the c-*mpl* (−135/−116) probe (*lane 2*), and their mobilities were almost the same with that detected by the positive control probe (*lane 7*). These complexes were abolished by the WT competitor (Fig. 2*A*, *lanes 3* and *8*) but not by the MT competitor (*lanes 4* and *9*). Furthermore, these complexes were supershifted by the anti-AML1 Ab (Fig. 2*A*, *lanes 5* and *10*). These data indicate that these complexes were formed in a sequence-specific manner and contained AML1. To further test whether endogenous AML1 binds to the *c-mpl* promoter *in vivo*, we conducted ChIP assays using the anti-AML1 Ab. To obtain enough numbers of hema-

Tet$^+$ and Tet$^-$ medium in these clones, and several clones were subjected to further analyses.

Colony Assays—Two days after retrovirus infection, GFP$^+$ cells (1000 cells/35-mm dish) were cultured in the methylcellulose media M3234 (Stem Cell Technologies, Vancouver, British Columbia, Canada) containing the indicated cytokines. The number of CFU-GM was counted on day 7 and those of BFU-E and CFU-GEMM on day 12.

RESULTS

Function of AML1b on c-mpl Promoter Activity—To examine the effect of AML1 on TPO/c-Mpl-mediated signaling, we initially examined whether AML1 transcriptionally regulates the expression of c-*mpl*. For this purpose, we performed luciferase assays with the −724 construct, a reporter gene containing the

Downloaded from www.jbc.org at OSAKA UNIVERSITY on February 1, 2009

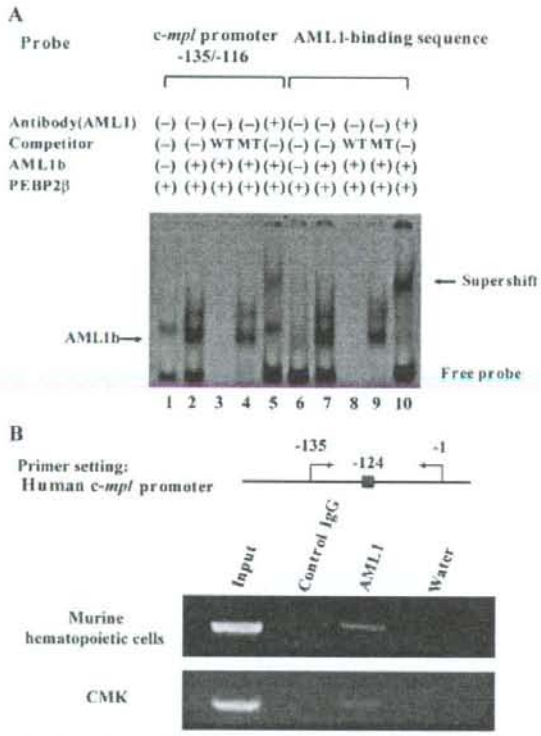

FIGURE 2. **Analysis of the responsive element to AML1b in the c-*mpl* promoter.** *A*, EMSA was performed with the probe containing putative AML1-binding sequence in the human c-*mpl* promoter or known AML1-binding sequence (positive control). Nuclear extract was isolated from 293T cells transfected with the indicated genes and subjected to EMSA. In competition assays, a 1000-fold molar excess of unlabeled wild-type or mutant competitor oligonucleotide was added to the binding mixture. *B*, location of AML1-binding site and the primer set in the c-*mpl* promoter utilized for the ChIP assay are indicated. The nuclear extract was isolated from primary cultured murine hematopoietic cells and CMK cells, and the chromatin was sonicated. Then AML1-DNA-binding complexes were immunoprecipitated with the anti-AML1 Ab (N-20) or control goat IgG. The immunoprecipitated DNA was eluted and subjected to the PCR analyses. PCR products were electrophoresed on agarose gels and visualized with SYBR Green staining.

topoietic cells, we separated Lin^- cells and cultured with mIL-3 and hTPO for 3 days. Nuclear extracts were isolated from 1×10^7 cultured cells. As shown in Fig. 2*B*, the c-*mpl* promoter, including the proximal AML1-binding site, was immunoprecipitated by the anti-AML1 Ab but not by control IgG (Fig. 2*B*). Similar results were also observed using the nuclear extract obtained from a human megakaryocytic cell line CMK (Fig. 2*B*). Together, these data indicate that endogenous AML1 bind to the proximal AML1-binding site in the c-*mpl* promoter and suggest that AML1 might regulate its transcription.

AML1dC Dominant-negatively Suppresses AML1 Function—Next, we examined the effects of a mutant of AML1b, AML1dC, on the c-*mpl* promoter activity. AML1dC is a C-terminal deletion mutant of AML1b (Fig. 3*A*), which was originally identified in a patient with MDS (30). Harada *et al.* (30) reported that this mutant suppressed transactivation activity of AML1 for macrophage colony-stimulating factor receptor. As was the case with the macrophage colony-stimulating factor receptor, AML1dC dose-dependently suppressed AML1b/PEBP2β-induced c-*mpl* promoter activity in 293T cells as efficiently as AML1-MTG8, which is known to act as a dominant-negative repressor of AML1 (Fig. 3*B*). To clarify how AML1dC inhibits AML1 activity, we performed EMSA with the c-*mpl* (−135/−116) probe. As shown in Fig. 3C, only 2.5 μg of cotransfected AML1dC was able to effectively cancel the DNA-binding complex formed by 10 μg of transfected wild-type AML1b, which was more prominent when 10 μg of AML1dC was cotransfected (Fig. 3C, *lanes 3* and *4*). These results suggest that AML1dC dominant-negatively suppresses the function of AML1 by inhibiting its DNA binding activity.

AML1dC Enhances c-Mpl Expression in Hematopoietic Stem/Progenitor Cells—Because TPO/c-Mpl signaling plays an important role in the proliferation and survival of hematopoietic stem/progenitor cells (33, 34), we next examined the function of AML1 in the c-Mpl regulation in hematopoietic stem/progenitor cells. For this purpose, we transduced AML1dC and AML1b into murine KSL cells with a retrovirus system (Fig. 4*A*). Two days after retrovirus infection, we sorted retrovirus-transduced cells, which are detected by the GFP expression, and performed RT-PCR analysis. Unexpectedly, in contrast to the result of luciferase assays in 293T and HeLa cells that suggests AML1 positively regulates the c-*mpl* expression, AML1dC-transduced cells expressed c-*mpl* mRNA more abundantly than mock-transduced cells in several repeated experiments (representative result is shown in Fig. 4*B*). In accord with this result, FACS analysis showed that the c-Mpl was more intensely expressed in AML1dC-transduced cells than in mock-transduced cells (mean fluorescent intensity, AMLdC 79.8 *versus* Mock 61.5) (Fig. 4*C*). On the other hand, c-*mpl* mRNA and cell-surface c-Mpl expression were suppressed in AML1b-transduced cells than those in Mock-transduced cells (mean fluorescent intensity: AMLb 49.0 *versus* Mock 61.5) (Fig. 4, *B* and *C*).

AML1dC Enhances c-Mpl Expression in Hematopoietic Cells That Derived from Murine ES Cells—To further explore the effects of AML1dC on the c-Mpl expression during the development of hematopoietic stem/progenitor cells, we utilized the Tet-Off system in the OP9 system. In the OP9 system, after deprivation of leukemia inhibitory factor from the culture medium, Flk-1$^+$ hemangioblasts that have both the potential to develop into hematopoietic cells and endothelial cells develop from ES cells after 4.5 days, and definitive hematopoietic stem/progenitor cells appear after 8.5 days (Fig. 5*A*) (42, 43). After sorting Flk-1$^+$ cells on day 4.5, we inducibly expressed AML1dC by depriving Tet from the culture medium, cultured for 4 days, and performed FACS analysis on day 8.5. After the culture with Tet, 50.5% of AML1dC-transduced ES cells were positive for c-Mpl in the GFP-negative fraction (Fig. 5*B, upper left panel*). In contrast, after the culture without Tet, 77.0% of AML1dC-transduced ES cells were positive for c-Mpl in the GFP-positive fraction (Fig. 5*B, upper right panel*). Similar results were obtained in other clones of AML1dC (data not shown). Tet deprivation by itself did not influence c-Mpl expression in mock-transduced ES cells (data not shown). Together with the results obtained from AML1dC- and

Downloaded from www.jbc.org at OSAKA UNIVERSITY on February 1, 2009

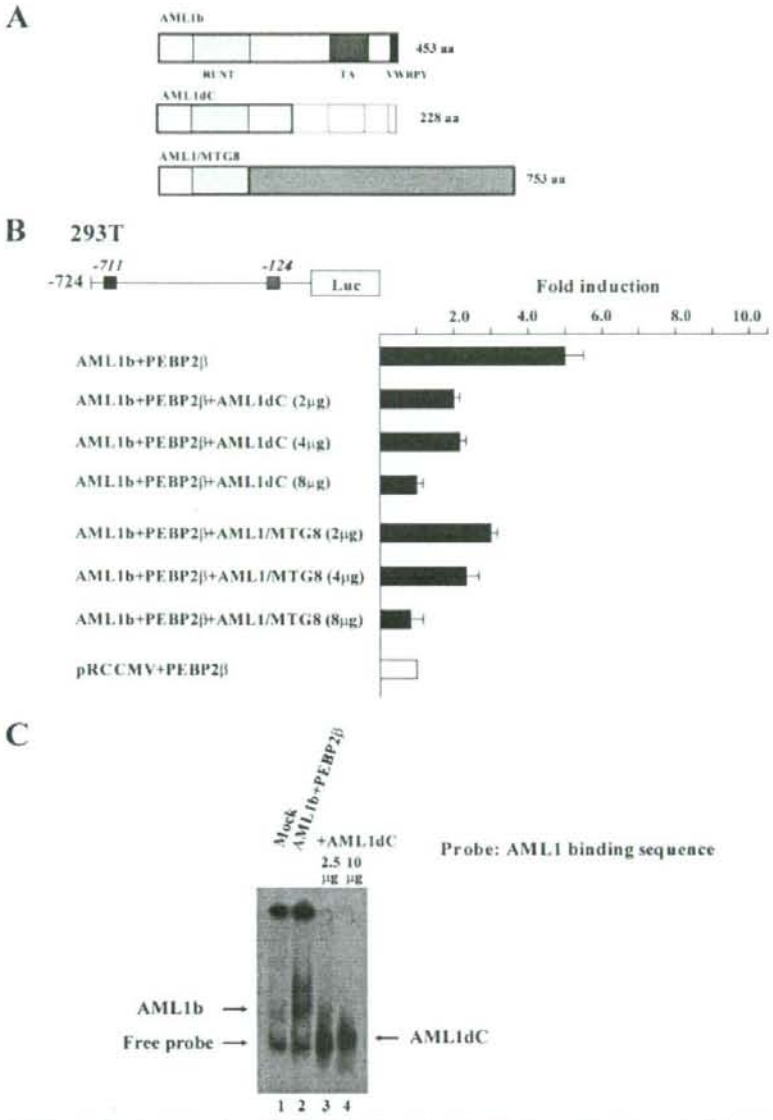

FIGURE 3. **AML1dC dominant-negatively suppresses AML1 function.** *A, horizontal bars* show WT AML1b (453 amino acids (*aa*)), C-terminal deletion mutant of AML1b (288 amino acids), and AML1/MTG8 (753 amino acids). In the case of AML1dC, the insertion of ACCGT into 669–670 causes frameshift mutation and results in truncation of WT AML1b. *RUNT* indicates the runt domain; *TA* indicates the transactivation domain; *VWRPY* indicates the VWRPY motif. *B*, 293T cells were transfected with 2 μg of AML1b, PEBP2β, and indicated doses of AML1dC or AML1/MTG8. The results are shown as the means ± S.D. of triplicate cultures. *C*, EMSA was performed with the probe containing AML1-binding sequence. Nuclear extracts were isolated from 293T cells transfected with empty vector (10 μg) or AML1b (10 μg), PEBP2β (10 μg), and indicated doses of AML1dC.

AML1b-transduced KSL cells, these results indicate that wild-type AML1 is a negative regulator of the c-*mpl* transcription in hematopoietic stem/progenitor cells.

Haploinsufficiency of AML1 Also Enhances c-Mpl Expression in ES-derived Hematopoietic Cells—AML1dC might influence the expression of c-Mpl on hematopoietic stem/progenitor cells not only as a dominant-negative mutant but also through the unknown mechanisms. So, it is important to examine the expression of c-Mpl on hematopoietic stem/progenitor cells, in which the expression of AML1 was simply reduced. For this purpose, we developed hematopoietic stem/progenitor cells from murine AML1$^{+/-}$ ES cells and examined the c-Mpl expression on these cells, because AML1-null-ES cells cannot differentiate into definitive hematopoietic cells (47). As a result, we found that early hematopoietic cells that derived from AML1$^{+/-}$ ES cells expressed c-Mpl more intensively than those that developed from WT ES cells (mean fluorescent intensity, AML1$^{+/-}$ 129.8 *versus* WT 27.0) (Fig. 5*C*). This result again suggests that AML1 is a negative regulator of c-Mpl expression in hematopoietic stem/progenitor cells.

AML1dC Does Not Influence the c-Mpl Expression in Megakaryocytes or Their Maturation—Except for immature hematopoietic cells, c-Mpl is exclusively expressed on megakaryocytic cells and plays essential roles in megakaryopoiesis and subsequent platelet production. So we next analyzed the effects of AML1dC on megakaryocytic maturation and the c-Mpl expression on mature megakaryocytes. For this purpose, we cultured AML1dC-transduced ES clones in the presence of TPO for 12.5 days (Fig. 5*D*). On day 12.5, morphologic analysis showed that AML1dC-transduced ES cells were able to possess polyploid nucleus, which is characteristic of mature megakaryocytes, regardless of the presence or absence of Tet (Fig. 5*D*). Also, FACS analysis on day 12.5 showed that Tet deprivation neither inhibited polyploidization of megakaryocytes (Fig. 5*E*) nor their c-Mpl expression (Fig. 5*B*, *lower panels*) in AML1dC-transduced ES cells.

AML1 Forms Different Transcriptional Complex on the c-mpl Promoter in Hematopoietic Stem/Progenitor Cells and Megakaryocytes—Our findings suggested AML1 differentially regulates the c-Mpl expression in hematopoietic stem/progenitor cells and megakaryocytic cells. Because AML1 forms a

Downloaded from www.jbc.org at OSAKA UNIVERSITY on February 1, 2009

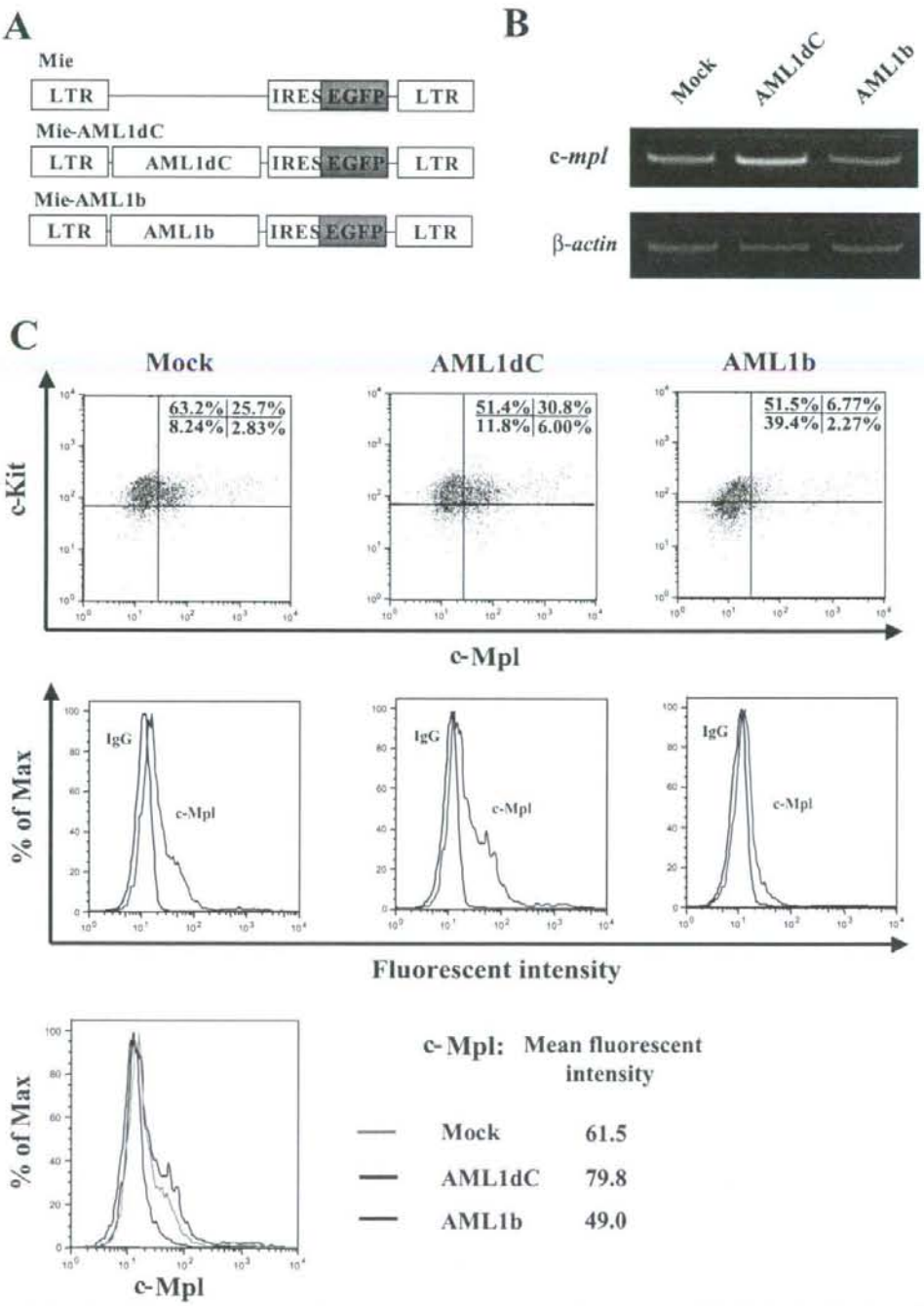

FIGURE 4. **Analysis of the c-Mpl expression in murine hematopoietic stem/progenitor cells.** *A*, structure of Mie (Mock), Mie-AML1dC, and Mie-AML1b retroviruses. *B*, 2 days after retroviral transfection, GFP$^+$ cells were sorted and subjected to RT-PCR to examine the expression of c-*mpl* and β-actin mRNA. *C*, at the same point, the surface phenotype of GFP$^+$ fraction of Mie, Mie-AML1dC, and Mie-AML1b-transduced cells was examined by FACS. Dot plots of cell-surface expressions of c-Kit and c-Mpl (*upper panels*) are shown. Histogram plots and mean fluorescent intensities of c-Mpl expression (*middle* and *lower panels*) are shown. *LTR*, long terminal repeat; *IRES*, internal ribosome entry site.

Downloaded from www.jbc.org at OSAKA UNIVERSITY on February 1, 2009

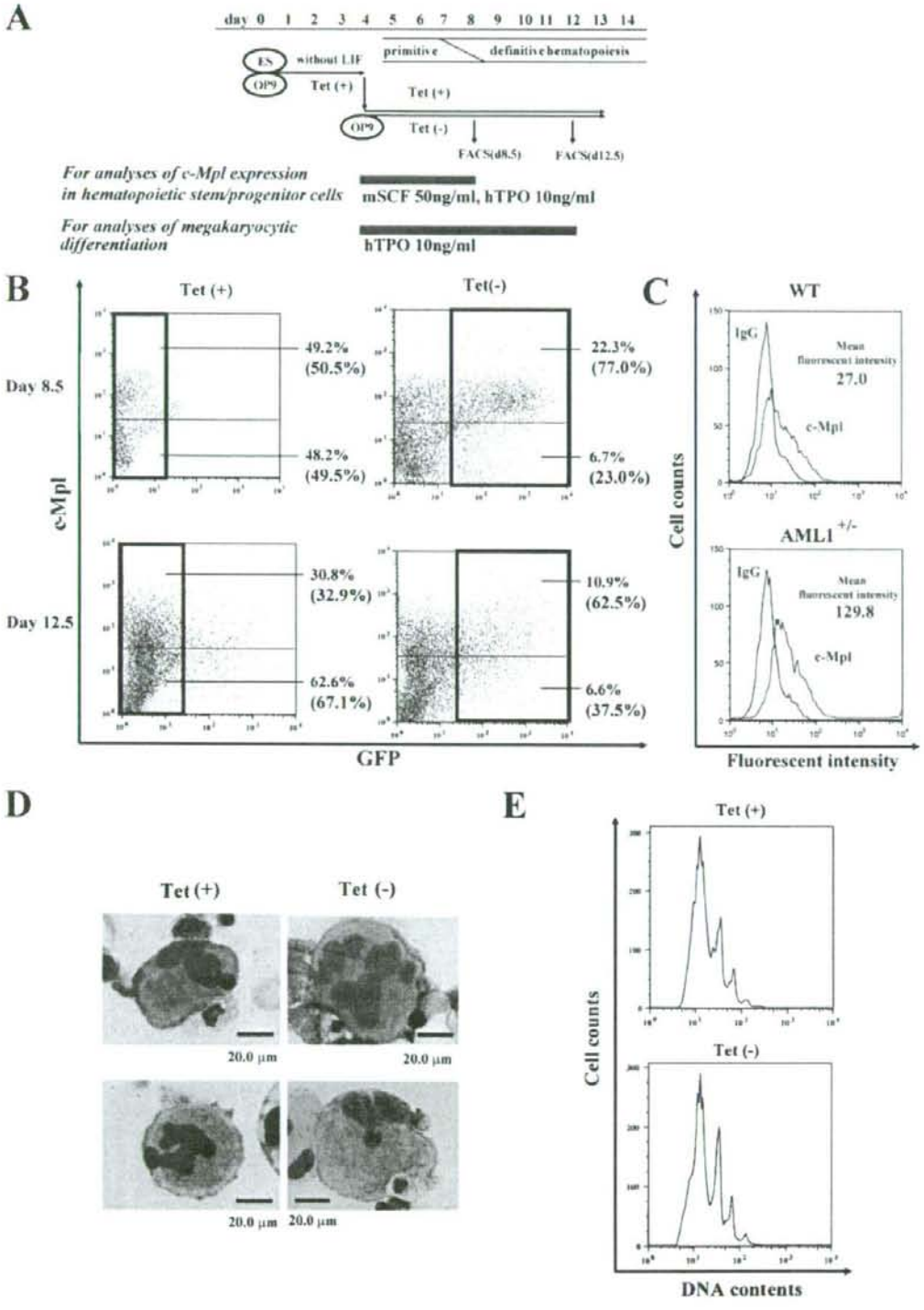

Downloaded from www.jbc.org at OSAKA UNIVERSITY on February 1, 2009

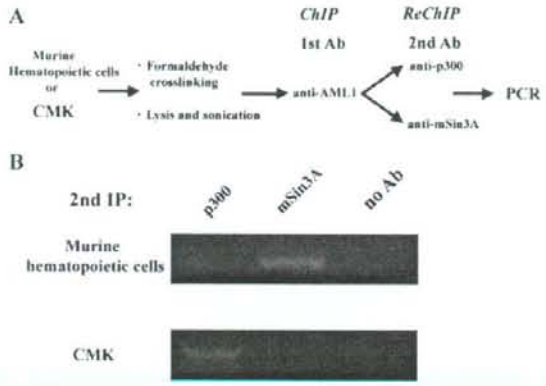

FIGURE 6. **AML1 forms different transcriptional complexes on the c-*mpl* promoter in hematopoietic stem/progenitor cells and megakaryocytes.** *A*, experimental design of ChIP-ReChIP assays. Murine Lin$^-$Sca1$^+$ cells were cultured for 3 days with mSCF (50 ng/ml), mIL-3 (10 ng/ml), and hTPO (50 ng/ml). These cultured cells and CMK cells were cross-linked and subjected to the ChIP-ReChIP assays. *B*, after the second immunoprecipitation (*IP*), PCR analyses were performed using the primer set shown in Fig. 2 with the eluted DNA as a template.

transcriptional complex with various molecules, we hypothesized that AML1 may change the binding partner included in the transcriptional complex, thereby regulating the c-*mpl* promoter either positively or negatively according to cell types. To assess this hypothesis, we performed ChIP-ReChIP assays. Nuclear extracts were prepared from 3-day-cultured Lin$^-$Sca1$^+$ cells and CMK cells. After the first ChIP with the AML1 Ab, the eluted samples, including the transcriptional complex of AML1, were re-immunoprecipitated by the anti-p300 Ab and anti-mSin3A Ab respectively (Fig. 6*A*). As shown in Fig. 6*B*, *upper panel*, the anti-mSin3A Ab but not the anti-p300 Ab immunoprecipitated the c-*mpl* promoter from the transcriptional complex of AML1 obtained from Lin$^-$Sca1$^+$ cells. In contrast, the c-*mpl* promoter was immunoprecipitated by the anti-p300 Ab but not by the anti-mSin3A Ab from the transcriptional complex of AML1 isolated from CMK cells (Fig. 6*B*). These results suggest that AML1 represses the c-*mpl* promoter by forming a complex with a transcriptional corepressor mSin3A in hematopoietic stem/progenitor cells, although it activates the c-*mpl* promoter by forming a complex with a transcriptional activator p300 in megakaryocytic CMK cells.

AML1dC Enhances TPO Signaling and TPO-dependent Colony Forming Activity—To assess the biologic significance of the AML1dC-enhanced c-Mpl expression in hematopoietic stem/progenitor cells, we initially compared TPO-induced tyrosine phosphorylation of STAT5 between AML1dC- and Mock-transduced KSL cells by flow cytometry. As a result, we found that the stimulation with TPO for 15 min activated STAT5 more effectively in AML1dC-transduced cells than in Mock-transduced cells (% of activated cells: AML1dC 51.8% *versus* Mock 32.2%) (Fig. 7*A*). Meanwhile, TPO-induced STAT5 activation in AML1b-transduced cells was distinctly attenuated compared with Mock-transduced cells (% of activated cells, AML1b 11.1% *versus* Mock 32.2%). Also, we performed colony assays using these cells under several conditions with or without TPO. As shown in Fig. 7*B*, although AML1dC- and Mock-transduced KSL cells developed almost equivalent numbers of hematopoietic colonies in the absence of TPO, AML1dC-transduced KSL cells yielded more and larger colonies than Mock-transduced KSL cells in the presence of TPO. In particular, CFU-GEMM was formed from AML1dC-transduced KSL cells but not from Mock-transduced KSL cells. These results suggest that the augmented c-Mpl expression by AML1dC led to the enhanced proliferation (in part, self-renewal) and survival of KSLs through the TPO/c-Mpl signaling (Fig. 7*B*).

DISCUSSION

Because both AML1 and TPO/c-Mpl signaling play important roles in the growth of HSCs and megakaryopoiesis, we assumed that AML1 might regulate TPO/c-Mpl signaling. Also, in a recent paper, Heller *et al.* (31) reported that platelet surface c-Mpl expression was decreased in FPD/AML patients, suggesting that AML1 would augment c-Mpl expression in megakaryocytes. To clarify this relationship, in this study we performed luciferase assays, EMSA, and ChIP assays with the c-*mpl* promoter. As a result, we found that AML1 directly binds to the proximal AML-binding sequence between −137 and −122 bp of the c-*mpl* promoter, thereby regulating its activity. In agreement with the suggestive data by Heller *et al.* (31), AML1 activated the c-*mpl* promoter in luciferase assays using 293T cells and HeLa cells. However, the enforced expression of a dominant-negative form of AML1, AML1dC, in KSL cells by the retrovirus system enhanced c-Mpl expression in hematopoietic stem/progenitor cells and exogenous AML1b transduction into KSL cells and attenuated c-Mpl expression and TPO-induced STAT5 activation. Also, the induced expression of AML1dC during the development of hematopoietic cells in the OP9 system enhanced c-Mpl expression on hematopoietic stem/progenitor cells. Furthermore, early hematopoietic cells that derived from AML1$^{+/-}$ ES cells expressed c-Mpl more intensively than those that developed from WT ES cells. These results suggest that AML1 is a negative regulator of c-Mpl expression in these cells, which is opposite to its role in megakaryocytes. As for this inconsistent result observed in hematopoietic stem/progenitor cells, we speculate that AML1 would be able to regulate the c-*mpl* promoter both positively and negatively according to cell types. In fact, AML1 and its heterodimeric partner, PEBP2β, have been reported to form a

FIGURE 5. **Effects of AML1dC on c-Mpl expression on hematopoietic progenitor cells and megakaryocytes and megakaryopoiesis.** *A*, experimental design using the OP9 system. ES cells were deprived of leukemia inhibitory factor and cultured on OP9 cells for 4.5 days. Then Flk-1$^+$ cell were sorted, replated onto OP9 cells, and cultured with mSCF and hTPO (for the analysis of c-Mpl expression in hematopoietic stem/progenitor cells) or only hTPO (for the analysis of megakaryocytic differentiation) with or without Tet for the time indicated. *B*, c-Mpl expression of nonadherent cells was examined by the direct immunofluorescence method on day 8.5 and day 12.5. The percentage of each fraction is indicated. The relative frequency of GFP$^-$ fraction in cultured cells with Tet and the relative frequency of GFP$^+$ fraction in cultured cells without Tet were shown in *parentheses*. *C*, c-Mpl expression on early hematopoietic cells that derived from WT and AML1$^{+/-}$ ES cells on day 8.5. *D* and *E*, after 12.5-day cultures with TPO, megakaryocytic cells, which derived from ES cells expressing AML1dC, were subjected to morphological analysis (*D*), and DNA content analysis by propidium iodide staining (*E*).

Downloaded from www.jbc.org at OSAKA UNIVERSITY on February 1, 2009

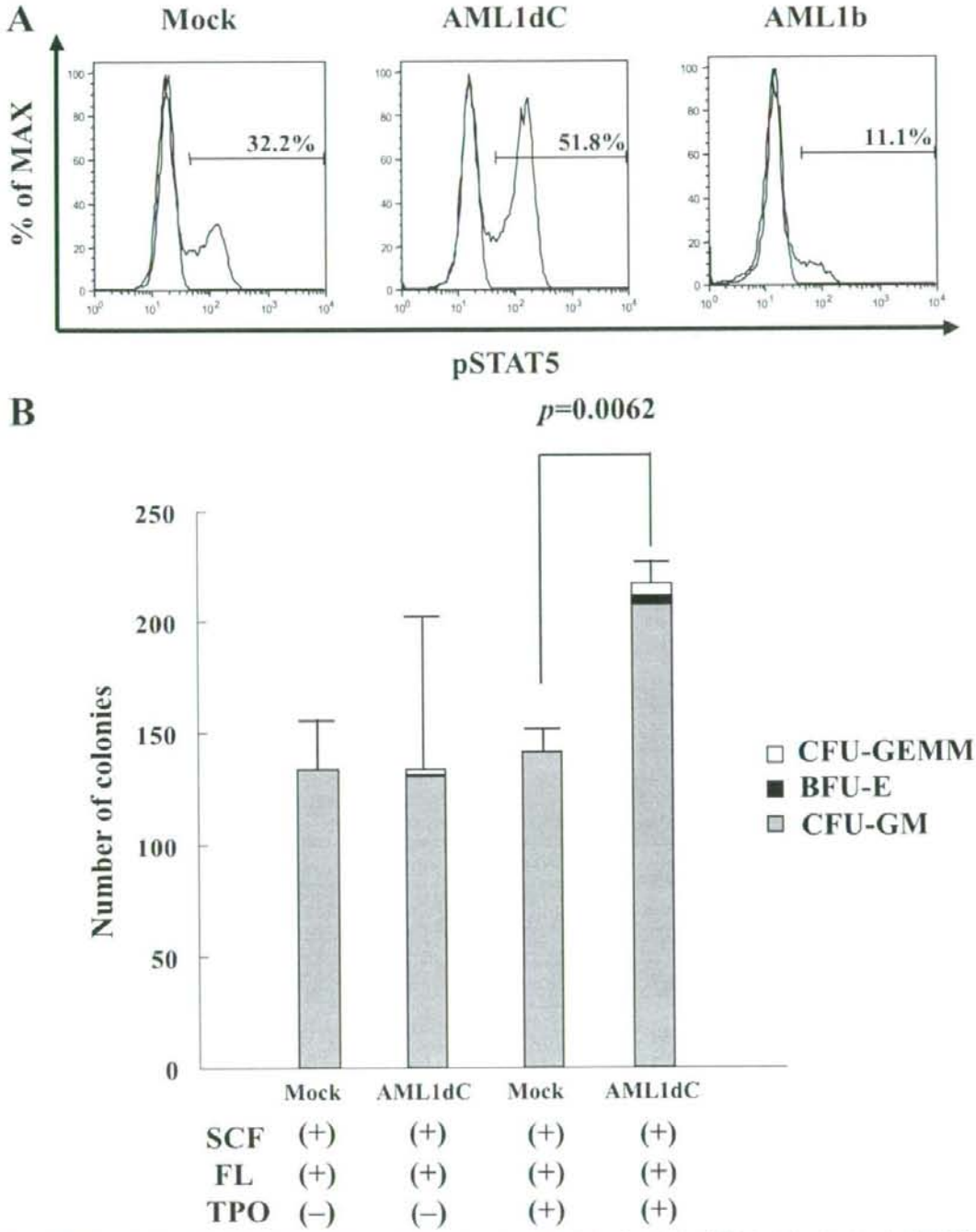

FIGURE 7. **AML1dC enhances TPO signaling and TPO-dependent colony forming activity.** *A*, after 15-min of TPO stimulation, tyrosine phosphorylation of STAT5 was examined by FACS in Mock-, AML1dC-, and AML1b-transduced cells, which are gated as a GFP$^+$ fraction. *Red line*, with TPO stimulation. *Blue line*, without TPO stimulation. *B*, 2 days after retrovirus infection, GFP$^+$ cells (1000 cells/dish) were seeded into the methylcellulose media with indicated cytokines. The number of CFU-GM was counted on day 7 and those of BFU-E and CFU-GEMM on day 12. The results are shown as mean ± S.D. of triplicate experiments. *CFU-GEMM (open square); BFU-E (closed square); CFU-GM (gray square).*

ASBMB The Journal of Biological Chemistry

Downloaded from www.jbc.org at OSAKA UNIVERSITY on February 1, 2009

transcriptional complex with various molecules and to change its function dependently on cell types. When AML1 forms a complex with p300/CBP and MOZ, this complex strongly stimulates AML1-mediated transcription (48). On the other hand, when AML1 combines with mSin3A, this complex works as a transcriptional repressor (49). In agreement with this speculation, we found that AML1 forms a complex with mSin3A on the c-*mpl* promoter in hematopoietic stem/progenitor cells, whereas it formed a complex with p300 on the same promoter in megakaryocytic cells (Fig. 6*B*). These results suggest that AML1 plays distinct roles in the regulation of the c-*mpl* promoter dependent on cell types by changing the binding partner.

In a previous paper, Ichikawa *et al.* (17) reported that conditional targeting of AML1 in adult mice led to the impaired polyploidization of megakaryocytes, resulting in the low platelet production. Also, patients with hereditary FPD/AML, which was caused by the heterozygous point mutations of the *AML1* gene or the *PEBP2β* gene revealed low platelet numbers in the peripheral blood (19). To clarify the roles of AML1 in megakaryocytic maturation, several studies have been performed. Consequently, Bernardin-Fried *et al.* (50) found that AML1 directly activates the cyclin D3 promoter, thereby enhancing DNA synthesis required for polyploidization. Also, Goldfarb and co-workers (51, 52) showed that AML1 binds to and activates the promoter of megakaryocyte-specific genes, αIIb integrin, and glycoprotein Ibα, in combination with a transcription factor specific for the erythroid/megakaryocyte lineage, GATA-1, thereby promoting phenotypic maturation of megakaryocytes (51, 52). Most AML1 mutations observed in FPD/AML and AML are clustered within the Runt domain in the N-terminal region (19, 53–55). Heterozygous Runt domain mutations show haploinsufficient phenotype because of their reduced DNA binding and PEBP2β binding (30, 53). On the other hand, because C-terminal deletion mutants of AML1 have enhanced DNA-binding potential, they strongly suppress wild-type AML1 function through the blocking of its DNA binding in a dominant-negative manner (30). In line with this result, we also found that AML1dC lacking the C-terminal amino acids 224–453 dominant-negatively suppressed DNA binding of WT AML1 in EMSA using nuclear extracts of 293T cells. However, in this study, we found that AML1dC scarcely influenced the morphology or polyploidization of megakaryocytes. This result seems to be at variance with previous reports indicating the importance of AML1 in megakaryopoiesis (as described above). However, because an apparent abnormality was not detected in megakaryopoiesis and platelet production in AML1 heterozygous knock-out mice (14), it was speculated that pure haploinsufficiency of AML1 would not impair maturation of megakaryocytes or platelet production. Although genuine haploinsufficiency of AML1 was observed in some cases, it was also speculated that a greater majority of mutant AML1 proteins are assumed to act in a dominant-negative manner (56). So, at present, it remains unknown to what degree AML1 activity must be suppressed to cause the defect in megakaryopoiesis. In addition, there is a possibility that although AML1dC was found to act as a dominant-negative suppressor of AML1 in 293T cells in this study, AML1dC protein might be far more labile than wild-type AML1 in megakaryocytes. Alternatively, it is also possible that AML1dC might reveal some unknown biologic effect on megakaryopoiesis in combination with other transcriptional regulators such as GATA-1. Although the precise mechanism remains to be clarified, our data suggest that AML1dC lacking the C-terminal amino acids 224–453 by itself would not be responsible for the impaired megakaryopoiesis in the original MDS patient. Further studies using several C-terminal mutants are required to clarify the roles of mutants of AML1 in impaired megakaryopoiesis in MDS patients.

Conditional deletion of AML1 in adult mice leads to the expansion of the HSC compartment and reduction of common lymphoid progenitors (CLPs) as well as impaired megakaryopoiesis (17, 18), suggesting that AML1 enhances differentiation of HSC toward the CLP compartment. Meanwhile, c-*mpl* mRNA is expressed on HSCs and common myeloid progenitors but not on CLPs (16). However, considering our result that AML1-deficient hematopoietic stem/progenitor cells are hyper-responsive to TPO because of the enhanced c-Mpl expression, these reports may simply indicate that AML1-deficient HSCs and common myeloid progenitors would overgrow as compared with CLPs in response to the TPO stimulation. Also, it was speculated that MDS stem cells harboring AML1dC might be hyper-responsive to TPO, leading to the accumulation of oxidative stress that causes second genetic abnormalities.

In conclusion, we show here that AML1 acts as a negative regulator of c-Mpl expression in hematopoietic stem/progenitor cells which is opposite to its role in megakaryocytes. Also, we found that hematopoietic stem/progenitor cells harboring AML1dC were hyperproliferative in response to TPO. Further studies focusing on the roles of various types of AML1 mutants would be useful to clarify the physiologic roles for AML1 and to understand the pathophysiology of MDS.

Acknowledgment—We thank Dr. Iwama for providing a vesicular stomatitis virus-G expression plasmid and technical advice.

REFERENCES

1. Miyoshi, H., Shimizu, H., Kozu, T., Maseki, N., Kaneko, Y., and Ohki, M. (1991) *Proc. Natl. Acad. Sci. U. S. A.* **88,** 10431–10434
2. Golub, T. R., Barker, G. F., Bohlander, S. K., Hebert, S. W., Ward, D. C., Bray-Ward, P., Morgan, E., Raimondi, S. C., Rowley, J. D., and Gilliland, D. G. (1995) *Proc. Natl. Acad. Sci. U. S. A.* **92,** 4917–4921
3. Osato, M. (2004) *Oncogene* **23,** 4284–4296
4. Sasaki, K., Yagi, H., Bronson, R. T., Tominaga, K., Matsunashi, T., Deguchi, K., Tani, Y., Kishimoto, T., and Komori, T. (1996) *Proc. Natl. Acad. Sci. U. S. A.* **93,** 12359–12363
5. Wang, Q., Stacy, T., Miller, J. D., Lewis, A. F., Gu, T. L., Huang, X., Bushweller, J. H., Bories, J. C., Alt, F. W., Ryan, G., Liu, P. P., Wynshaw-Boris, A., Binder, M., Marin-Padilla, M., Sharpe, A. H., and Speck, N. A. (1996) *Cell* **87,** 697–708
6. Niki, M., Okada, H., Takanu, H., Kuno, J., Tani, K., Hibino, H., Asanu, S., Ito, Y., Satake, M., and Noda, T. (1997) *Proc. Natl. Acad. Sci. U. S. A.* **94,** 5697–5702
7. Cameron, S., Taylor, D. S., TePas, E. C., Speck, N. A., and Mathey-Prevot, B. (1994) *Blood* **83,** 2851–2859
8. Otto, F., Lübbert, M., and Stock, M. (2003) *J. Cell. Biochem.* **89,** 9–18
9. Taniuchi, I., Osato, M., Egawa, T., Sunshine, M. J., Bae, S. C., Komori, T., Ito, Y., and Littman, D. R. (2002) *Cell* **111,** 621–633

Downloaded from www.jbc.org at OSAKA UNIVERSITY on February 1, 2009

10. Woolf, E., Xiao, C., Fainaru, O., Lotem, J., Rosen, D., Negreanu, V., Bernstein, Y., Goldenberg, D., Brenner, O., Berke, G., Levanon, D., and Groner, Y. (2003) *Proc. Natl. Acad. Sci. U. S. A.* **100,** 7731–7736
11. Takahashi, A., Satake, M., Yamaguchi-Iwai, Y., Bae, S. C., Lu, J., Maruyama, M., Zhang, Y. W., Oka, H., Arai, N., Arai, K., and Ito, Y. (1995) *Blood* **86,** 607–616
12. Zhang, D. E., Fujioka, K., Hetheringtun, C. J., Shapiro, L. H., Chen, H. M., Look, A. T., and Tenen, D. G. (1994) *Mol. Cell. Biol.* **14,** 8085–8095
13. Jiang, H., Zhang, F., Kurozu, T., and Peterlin, B. M. (2005) *Mol. Cell. Biol.* **25,** 10675–10683
14. Okuda, T., van Deursen, J., Hiebert, S. W., Grosveld, G., and Downing, J. R. (1996) *Cell* **84,** 321–330
15. North, T. E., de Bruijn, M. F., Stacy, T., Talebian, L., Lind, E., Robin, C., Binder, M., Dzierzak, E., and Speck, N. A. (2002) *Immunity* **16,** 661–672
16. Akashi, K., Traver, D., Miyamoto, T., and Weissman, I. L. (2000) *Nature* **404,** 193–197
17. Ichikawa, M., Asai, T., Chiba, S., Kurokawa, M., and Ogawa, S. (2004) *Nat. Med.* **10,** 299–304
18. Growney, J. D., Shigematsu, H., Li, Z., Lee, B. H., Adelsperger, J., Rowan, R., Curley, D. P., Kutok, J. L., Akashi, K., Williams, I. R., Speck, N. A., and Gilliland, D. G. (2005) *Blood* **106,** 494–504
19. Song, W. J., Sullivan, M. G., Legare, R. D., Hutchings, S., Tan, X., Kufrin, D., Ratajczak, J., Resende, I. C., Haworth, C., Hock, R., Loh, M., Felix, C., Roy, D. C., Busque, L., Kurnit, D., Willman, C., Gewirtz, A. M., Speck, N. A., Bushweller, J. H., Li, F. P., Gardiner, K., Poncz, M., Maris, J. M., and Gilliland, D. G. (1999) *Nat. Genet.* **23,** 166–175
20. Hirai, H. (2003) *Jpn. J. Clin. Oncol.* **33,** 153–160
21. Paquette, R. L., Landaw, E. M., Pierre, R. V., Kahan, J., Lübbert, M., Lazcano, O., Isaac, G., McCormick, F., and Koeffler, H. P. (1993) *Blood* **82,** 590–599
22. Yokota, S., Kiyoi, H., Nakao, M., Iwai, T., Misawa, S., Okuda, T., Sonoda, Y., Abe, T., Kahsima, K., Matsuo, Y., and Naoe, T. (1997) *Leukemia (Basingstoke)* **11,** 1605–1609
23. Uchida, T., Kinoshita, T., Nagai, H., Nakahara, Y., Saito, H., Hotta, T., and Murate, T. (1997) *Blood* **90,** 1403–1409
24. Quesnel, B., Guillerm, G., Vereecque, R., Wattel, E., Preudhomme, C., Bauters, F., Vanrumbeke, M., and Fenaux, P. (1998) *Blood* **91,** 2985–2990
25. Sugimoto, K., Hirano, H., Toyoshima, H., Chiba, S., Mano, H., Takaku, F., Yazaki, Y., and Hirai, H (1993) *Blood* **81,** 3022–3026
26. Russell, M., List, A., Greenberg, P., Woodward, S., Glinsmann, B., Parganas, E., Ihle, J., and Taetle, R. (1994) *Blood* **84,** 1243–1248
27. Willman, C. L., Sever, C. E., Pallavicini, M. G., Harada, H., Tanaka, N., Slovak, M. L., Yamamoto, H., Harada, K., Meeker, T. C., List, A. F., *et al.* (1993) *Science* **259,** 968–971
28. Harada, H., Harada, Y., Tanaka, H., Kimura, A., and Inaba, T. (2003) *Blood* **101,** 673–680
29. Yoneda-Kato, N., Look, A. T., Kirstein, M. N., Valentine, M. B., Raimondi, S. C., Cohen, K. J., Carroll A. J., and Morris, S. W. (1996) *Oncogene* **12,** 265–275
30. Harada, H., Harada, Y., Niimi, H., Kyo, T., Kimura, A., and Inaba, T. (2004) *Blood* **103,** 2316–2324
31. Heller, P. G., Glembotsky, A. C., Gandhi, M. J., Cummings, C. J., Pirola, C. J., Marta, R. F., Kornblihtt, L. I., Drachman, J. G., and Molinas, F. C. (2005) *Blood* **105,** 4664–4670
32. Kaushansky, K., Lok, S., Holly, R. D., Broudy, V. C., Lin, N., Bailey, M. C., Forstrom, J. W., Buddle, M. M., Oort, P. J., Hagen F. S., Roth, G. J., Papayannopoulou, T., and Foster, D. C. (1994) *Nature* **369,** 568–571
33. Solar, G. P., Kerr, W. G., Zeigler, F. C., Hess, D., Donahue, C., de Sauvage, F. J., and Eaton, D. L. (1998) *Blood* **92,** 4–10
34. Fox, N., Priestley, G., Papayannopoulou, T., and Kaushansky, K. (2002) *J. Clin. Investig.* **110,** 389–394
35. Shimizu, K., Kitabayashi, I., Kamada, N., Abe, T., Maseki, N., Suzukawa, K., and Ohki, M. (2000) *Blood* **96,** 288–296
36. Gu, T. L., Goetz, T. L., Graves, B. J., and Speck, N. A. (2000) *Mol. Cell. Biol.* **20,** 91–103
37. Matsumura, I., Kitamura, T., Wakao, H., Tanaka, H., Hashimoto, K., Albanese, C., Downward, J., Pestell, R. G., and Kanakura, Y. (1999) *EMBO J.* **18,** 1367–1377
38. Satoh, Y., Matsumura, I., Tanaka, H., Ezoe, S., Sugahara, H., Mizuki, M., Shibayama, H., Ishiko, E., Ishiko, J., Nakajima, K., and Kanakura, Y. (2004) *J. Biol. Chem.* **279,** 24986–24993
39. Meyers, S., Downing, J. R., and Hiebert, S. W. (1993) *Mol. Cell. Biol.* **13,** 6336–6345
40. Jalvy, S., Renault, M. A., Lam Shang Leen, L., Belloc, I., Reynaud, A., Gadeau, A. P., and Desgranges, C. (2007) *Circ. Res.* **100,** 1292–1299
41. Wei, X., Xu, H., and Kufe, D. (2007) *Cancer Res.* **67,** 1853–1858
42. Nakano, T., Kodama, H., and Honjo, T. (1994) *Science* **265,** 1098–1101
43. Niwa, H., Burdon, T., Chambers, I., and Smith, A. (1998) *Genes Dev.* **12,** 2048–2060
44. Era, T., and Witte, O. N. (2000) *Proc. Natl. Acad. Sci. U. S. A.* **97,** 1737–1742
45. Nakata, S., Matsumura, I., Tanaka, H., Ezoe, S., Satoh, Y., Ishikawa, J., Era, T., and Kanakura, Y. (2004) *J. Biol. Chem.* **279,** 55578–55586
46. Vangala, R. K., Heiss-Neumann, M. S., Rangatia, J. S., Singh, S. M., Schoch, C., Tenen, D. G., Hiddemann, W., and Behre, G. (2003) *Blood* **101,** 270–277
47. Okuda, T., Takeda, K., Fujita, Y., Nishimura, M., Yagyu, S., Yoshida, M., Akira, S., Downing, J. R., and Abe, T. (2000) *Mol. Cell. Biol.* **20,** 319–328
48. Kitabayashi, I., Aikawa, Y., Nguyen, L. A., Yokoyama, A., and Ohki, M. (2001) *EMBO J.* **20,** 7184–7196
49. Lutterback, B., Westendorf, J. J., Linggi, B., Isaac, S., Seto, E., and Hiebert, S. W. (2000) *J. Biol. Chem.* **275,** 651–656
50. Bernardin-Fried, F., Kummalue, T., Leijen, S., Collector, M. I., Ravid, K., and Friedman, A. D. (2004) *J. Biol. Chem.* **279,** 15678–15687
51. Elagib, K. E., and Goldfarb, A. N. (2007) *Crit. Rev. Eukaryotic Gene Expression* **17,** 271–280
52. Elagib, K. E., Racke, F. K., Mogass, M., Khetawat, R., Delehanty, L. L., and Goldfarb, A. N. (2003) *Blood* **101,** 4333–4341
53. Michaud, J., Wu, F., Osato, M., Cottles, G. M., Yanagida, M., Asou, N., Shigesada, K., Ito, Y., Benson, K. F., Raskind, W. H., Rossier, C., Antonarakis, S. E., Israels, S., McNicol, A., Weiss, H., Horwitz, M., and Scott, H. S. (2002) *Blood* **99,** 1364–1372
54. Osato, M., Asou, N., Abdalla, E., Hoshino, K., Yamasaki, H., Okubo, T., Suzushima, H., Takatsuki, K., Kanno, T., Shigesada, K., and Ito, Y. (1999) *Blood* **93,** 1817–1824
55. Preudhomme, C., Warot-Loze, D., Roumier, C., Grardel-Duflos, N., Garand, R., Lai, J. L., Dastugue, N., Macintyre, E., Denis, C., Bauters, F., Kerckaert, J. P., Cosson, A., and Fenaux, P. (2000) *Blood* **96,** 2862–2869
56. Osato, M., Yanagida, M., Shigesada, K., and Ito, Y. (2001) *Int. J. Hematol.* **74,** 245–251
57. Kimura, S., Roberts, A. W., Metcalf, D., and Alexander, W. S. (1998) *Proc. Natl. Acad. Sci. U. S. A.* **95,** 1195–1200

Downloaded from www.jbc.org at OSAKA UNIVERSITY on February 1, 2009